# LUND UNIVERSITY

**Model Based Optimization of a Complete Diesel Engine/SCR System**

Ericson, Claes

2009

*Citation for published version (APA):*
Ericson, C. (2009). *Model Based Optimization of a Complete Diesel Engine/SCR System*. [Doctoral Thesis (compilation), Combustion Engines]. Division of Combustion Engines, Lund Institute of Technology.

*Total number of authors:*
1

# Model Based Optimization of a Complete Diesel Engine/SCR System

**Claes Ericson**

Division of Combustion Engines

Department of Energy Sciences

Faculty of Engineering

Lund University

Doctoral Thesis

## LUND UNIVERSITY

# List of papers

## Paper I
**Transient emission predictions with quasi stationary models**
C. Ericson, B. Westerberg and R. Egnell
SAE Technical papers 2005-01-3852, 2005.

## Paper II
**Modelling diesel engine combustion and $NO_x$ formation for model based control and simulation of engine and exhaust aftertreatment system**
C. Ericson, M. Andersson, R. Egnell and B. Westerberg
SAE Technical papers 2006-01-0687, 2006.

## Paper III
**A state-space simplified SCR catalyst model for real time applications**
C. Ericson, I. Odenbrand and B. Westerberg
SAE Technical papers 2008-01-0616, 2008.

## Paper IV
**Characterisation and Model Based Optimization of a Complete Diesel Engine/SCR System**
C. Ericson, R. Egnell, I. Odenbrand and B. Westerberg
SAE Technical papers 2009-01-0896, 2009.

## Paper V
**Model Predictive Control of a Combined EGR/SCR HD Diesel Engine**
C. Ericson, R. Egnell, I. Odenbrand and B. Westerberg
Abstract submitted to SAE World Congress 2010.

# Other publications

**$NO_x$ Modelling of a Complete Diesel Engine / SCR System**
C. Ericson
Licentiate thesis, Division of Combustion Engines, ISRN LUTMDN/TMHP-07/7047, Department of Energy Sciences, LTH, Lund University, 2007.

**Mean value modelling of a poppet valve EGR-system**
C. Ericson
Masters thesis, Vehicular Systems, Department of Electrical Engineering, Linköping University, 2004.

# Abstract

Achieving upcoming emissions legislation (Euro VI) for heavy trucks is a serious challenge for the manufacturers. Apart from the increasingly strict limits on nitrogen oxides ($NO_x$) and particulate emissions (PM), the limited amount of fossil fuels as well as alarming climate changes simultaneously drives the demand for low $CO_2$ emissions. A likely solution to meet upcoming $NO_x$ limits is to use a combination of exhaust gas recirculation (EGR) and selective catalytic reduction (SCR). Combining these two technologies poses new challenges and possibilities when it comes to optimization and calibration.

Using a complete system approach, i.e. considering the engine and the aftertreatment system as a single unit, is important in order to achieve a good balance between regulated emissions and $CO_2$/fuel consumption. Optimizing the complete system is a tedious task; first there are a large number of variables which affect both emissions and fuel consumption (injection timing, EGR rate, urea dosing, injection pressure, pilot/post injections for example). Secondly, the SCR catalyst has substantially slower dynamics than the diesel engine and the rest of the system, making the optimization problem time dependent.

A novel approach to solve this problem is to use model based optimization which is the topic of this thesis. The first step involves developing computationally efficient models of the diesel engine, exhaust system and SCR catalyst.

The engine model consists of a quasi steady gas exchange model and a zero dimensional combustion and $NO_x$ formation model. The combustion model uses a two zone concept and the $NO_x$ formation is calculated according to the Zeldovich mechanism. The exhaust system model is a dynamic mean value model and considers convective heat transfer only. The SCR catalyst model is based on a state space concept and uses customized ODE solvers to allow long time step lengths. All sub models are optimized for computational efficiency and the complete model has a simulation performance of >10 times real time on a standard PC. The agreement with measurements is excellent; specific $NO_x$ engine out is predicted with a -8.5% relative error and $NO_x$ conversion over the SCR catalyst is underpredicted with 4.0 %.

The optimization problem is formulated to minimize brake specific fuel consumption including urea cost while maintaining $NO_x$ and $NH_3$ emissions at Euro VI levels. The steady state optimization problem is solved in an efficient manner by using a simplified steady state solution of the SCR catalyst model. A non linear controller based on the MPC principle is developed to solve the optimization problem for transient sequences. An SQP-based optimization routine is used to solve the MPC optimization problem in each time step.

The controller is applied to the certification test cycles (WHSC/WHTC). In the WHSC, the peak $NH_3$ slip is reduced from 85 to 17 ppm while the fuel consumption is unchanged compared to the optimum steady state calibration. Equally good results are achieved in the WHTC. Compared to a conservative steady state calibration with $NO_x$ and average $NH_3$ emissions on the same level, peak $NH_3$ slip is reduced from 102 to 47 ppm, and fuel consumption is improved by 1.5%.

# Svensk sammanfattning

## *Modellbaserad Optimering av ett Komplett Dieselmotor / SCR-System*
## *– en populärvetenskaplig sammanfattning*

Denna avhandling beskriver metoder för att optimera balansen mellan utsläppen av kväveoxider, $NO_x$, och koldioxid, $CO_2$, för en dieselmotor i en tung lastbil. $NO_x$ är skadligt för både hälsa och miljö och $CO_2$ är en växthusgas. Under det senaste decenniet har utsläppen av $NO_x$ från lastbilar minskat med omkring 70 % genom ny teknik som drivits fram med lagstiftning. Dagens lagkrav, Euro V, infördes 2008 och 2013 kommer Euro VI att införas som kräver en minskning av $NO_x$ med ytterligare minst 75 %. Samtidigt efterfrågar köparna av lastbilar en låg bränsleförbrukning och därmed indirekt låga utsläpp av $CO_2$. Generellt kan sägas för en dieselmotor att låg bränsleförbrukning står i motsats till låga $NO_x$-utsläpp.

I en dieselmotor kan man minska bildandet av $NO_x$ vid förbränningen genom att justera dieselinsprutningen eller återcirkulera avgaser. Ett alternativ är att minska mängden $NO_x$ i en katalysator som sitter monterad efter motorn. Katalysatorn använder principen selektiv katalytisk reduktion (SCR). För framtida lagkrav (Euro VI) kommer förmodligen en kombination av motoråtgärder och användandet av en katalysator att behövas. För att uppnå den optimala balansen mellan $NO_x$-utsläpp och bränsleförbrukning är det viktigt att man har ett helhetskoncept. Med andra ord måste motorn och katalysatorn optimeras tillsammans som en helhet.

En stor mängd parametrar styr både bränsleförbrukningen och bildandet av $NO_x$ i dieselmotorn. Dessutom så är katalysatorn känslig för temperatur; dess förmåga att reducera $NO_x$ sjunker snabbt vid låga temperaturer. Beroende på driftsfall så finns det alltså en mängd olika möjligheter att klara lagkraven för $NO_x$-utsläpp och svårigheten ligger då i att hitta den kombination som ger lägsta möjliga bränsleförbrukning. Samtidigt så måste hänsyn tas till att katalysatorn har en stor tröghet, vilket gör att den bästa inställningen i ett visst driftsfall beror på hur lastbilen har körts tidigare.

Metoderna som beskrivs bygger på modellbaserad optimering. Som första steg har matematiska modeller för bildandet av $NO_x$ i dieselmotorn och reduktionen av $NO_x$ i katalysatorn utvecklats. Målet är att minimera bränsleförbrukningen samtidigt som $NO_x$-utsläppen ligger under lagkravsnivån. Modellerna används för att studera vilka driftsfall som är mest avgörande för prestandan hos helheten motor plus katalysator. Utifrån den kunskapen formuleras ett optimeringsproblem.

Slutsatsen är att modellbaserad optimering är en bra metod för att optimera balansen mellan bränsleförbrukning och $NO_x$-utsläpp. Vid driftsfall då belastningen varierar snabbt kan bränsleförbrukningen minskas med upp till 1.5%. Det uppnås genom att reglera motorn och katalysatorn på ett sätt som tar hänsyn till trögheten i katalysatorn.

# Acknowledgements

# Notation and Acronyms

| | | |
|---|---|---|
| $A$ | [m²] | Current cylinder wall area |
| $A_{egr}$ | [m²] | EGR valve active flow area |
| $A_{exh.sys}$ | [m²] | Inner/outer wall area of exhaust system |
| $A_k$ | [m²] | Mass/heat transfer area, catalyst channel segment k |
| $A_s$ | [m²] | Catalyst wall cross sectional area |
| $B$ | [m] | Cylinder bore |
| $BMEP/IMEP$ | [bar] | Brake/Indicated Mean Effective Pressure |
| $c_i$ | [mole/m³] | Concentration of species i |
| $C_{diff}$ | [1/s] | Diffusion combustion heat release factor |
| $c_{i,eq}$ | [mole/m³] | Equilibrium concentration of species i |
| $c_{p,i}$ | [J/kg K] / [J/mol K] | Specific heat capacity of component i |
| $C_{rad}$ | [J/mol K⁴] | Parameter in radiative heat transfer expression |
| $c_{tot}$ | [mole/m³] | Total concentration |
| $C_{wo}$ | [1] | Constant in convective heat transfer expression |
| $C_X$ | [g/kWh] / [ppm] / [1] | Optimization constraint function X |
| $d$ | [m] | Catalyst channel width |
| $D_{eff,i}$ | [m²/s] | Effective diffusivity, specie i |
| $d_{exh.sys}$ | [m] | Diameter of the exhaust system |
| $D_i$ | [m²/s] | Diffusivity, specie i |
| $D_{K,i}$ | [m²/s] | Knudsen diffusivity, specie i |
| $d_P$ | [m] | Catalyst mean pore diameter |
| $D_{ref,i}$ | [m²/s] | Diffusivity at reference temperature, specie i |
| $E_{A,i}$ | [J/mole] | Activation energy, reaction i |
| $EQurea$ | [1] | Equivalent cost of urea |
| $f_{BSFC}$ | [g/kWh] | Brake specific fuel consumption |
| $f_D$ | [1] | Catalyst porosity-turtuosity factor |
| $f_{eq}$ | [K] | Temperature dissociation compensation |
| $F_{tot}$ | [mol/s] | Total molar flow |
| $FMEP/PMEP$ | [bar] | Friction/Pumping Mean Effective Pressure |
| $g_x$ | [1] | Black box function x |
| $h_c$ | [J/s m² K] | In-cylinder convective heat transfer coefficient |
| $h_{cve} / h_{cvi}$ | [J/s m² K] | External/internal convective heat transfer coefficient |
| $h_{gi}$ | [J/s m² K] | Generalized internal heat transfer coefficient |
| $h_k$ | [J/s m² K] | Catalyst heat transfer coefficient, segment K |
| $h_x$ | [J/kg] | Specific enthalpy of x |
| $H_{v,i}$ | [J/mol] | Heat of vaporization, specie i |
| $J_{trb}$ | [Nm s] | Turbocharger moment of inertia |
| $k_c$ | [m/s] | Catalyst film mass transfer coefficient |
| $K_{es}$ | [1/m⁴] | Restriction constant, exhaust system |
| $k_{0,i} / k_i$ | [m³/s]/[m³/s kg] /[mole/s kg] /[m⁶/mole s] | Preexponential factor/rate coefficient, reaction i |

| | | |
|---|---|---|
| $K_x$ | [1] | Constant x |
| $M$ | [Nm] | Torque |
| $m_{burn}$ | [kg] | Burned zone mass |
| $m_{exh.sys}$ | [kg] | Mass of the exhaust system |
| $m_{flame}$ | [kg] | Mass of freshly burned mass element (flame) |
| $M_i$ | [kg/mole] | Molar mass of specie i |
| $m_{s,k}$ | [kg] | Total mass solid material, catalyst channel segment k |
| $M_{trb}$, $M_{cmp}$ | [Nm] | Turbine/compressor torque |
| $n_i$ | [mole] | Number of moles, specie i |
| $\dot{n}_i$ | [mole/s] | Molar flow, specie i |
| $N_C$ | [mole/kg] | Specific number of active sites of catalyst |
| $N_{cyl}$ | [1] | Number of cylinders |
| $N_{eng}$ | [rpm] | Engine speed |
| $Nu$ / $Nu_\infty$ | [1] | Nusselt number / Asymptotic Nusellt number |
| $p$ | [bar] | Cylinder pressure |
| $P$ | [kW] | Engine power |
| $p_{amb}$ | [bar] | Ambient pressure |
| $p_{es}$ | [bar] | Exhaust system pressure |
| $p_{evo}$ | [bar] | Cylinder pressure at exhaust valve opening |
| $p_{im}$, $p_{em}$ | [bar] | Intake/exhaust manifold pressure |
| $p_{max}$ | [bar] | Peak cylinder pressure |
| $p_{motored}$ | [bar] | Motored cylinder pressure |
| $p_{rail}$ | [bar] | Common rail (injection) pressure |
| $Q_{fuel,inj}$ / $Q_{fuel,inj,diff}$ | [J] | Injected fuel energy total / available for diffusion comb. |
| $Q_g$, $Q_n$ | [J] | Total gross/Net heat release |
| $Q_{g,premix}$ / $Q_{g,diff}$ | [J] | Premix/diffusion combustion heat release |
| $Q_{ht,conv}$ | [J] | Combustion convective heat loss |
| $Q_{ht,rad}$ | [J] | Combustion radiative heat loss |
| $q_k$ | [J/s m²] | Solid catalyst heat flux |
| $Q_{LHV}$ | [J] | Lower heating value |
| $Q_{premix,tot}$ | [J] | Total heat released during premixed combustion |
| $R$ | [J/kg K] / [J/mole K] | Specific/universal gas constant |
| $Re$ | [1] | Reynolds number |
| $r_i$ | [mole/s] / [mole/s kg] / [1/CAD] | Reaction rate, reaction i |
| $Sh$ / $Sh_\infty$ | [1] | Sherwood number / Asymptotic Sherwood number |
| $S_p$ | [m/s] | Mean piston speed |
| $t$ | [s] | Time |
| $T$ | [K] | Cylinder charge temperature |
| $t_{AEOI}$ | [s] | Time after end of injection |
| $T_{amb}$ | [K] | Ambient temperature |
| $T_{burn}$ | [K] | Burned zone temperature after dissociation compensation |
| $T_{burn,perf}$ | [K] | Burned zone temperature before dissociation compensation |

| Symbol | Units | Description |
|---|---|---|
| $T_{cat,in}$ | [K] | Exhaust temperature pre catalyst (with urea inj. comp.) |
| $T_{evo}$ | [K] | Cylinder charge temperature at exhaust valve opening |
| $T_{exh}$ | [K] | Exhaust temperature after engine |
| $T_{exp}$ | [K] | Expanded burned zone temp |
| $T_{flame,ad}$ | [K] | Adiabatic flame temperature |
| $T_{flame,ht}$ | [K] | Radiation compensated adiabatic flame temperature |
| $T_g$ | [K] | Gas bulk temperature |
| $T_{im}$, $T_{em}$ | [K] | Intake/exhaust manifold temperature |
| $t_{MPC}$ | [s] | MPC prediction horizon |
| $T_{precat}$ | [K] | Exhaust temperature pre catalyst |
| $T_{ref}$ | [K] | Reference temperature, diffusivity calculations |
| $T_s$ | [K] | Catalyst surface temperature |
| $T_{SOI}/T_{SOC}$ | [K] | Cylinder charge temperature at SOI/SOC |
| $T_{trb}$ | [K] | Temperature after turbine |
| $T_w$ | [K] | Exhaust system wall temperature |
| $T_{wall}$ | [K] | Combustion chamber wall temperature |
| $u$ | [m/s] | Average in-cylinder gas velocity |
| $u_{channel}$ | [m/s] | Gas velocity in the catalyst channels |
| $u_{egr}$ / $u_{vgt}$ | [V] | EGR valve/VGT actuator control signal |
| $u_f$ | [m/s] | Fuel spray velocity |
| $V$ | [m³] | Current cylinder volume |
| $V_{disp}$ | [m³] | Swept cylinder volume |
| $V_{em}/V_{im}$ | [m³] | Volume of exhaust/intake manifold |
| $V_{es}$ | [m³] | Exhaust system volume |
| $V_{precat}$ | [m³] | Volume between urea injector and catalyst substrate |
| $W_{air}$ | [kg/s] | Air mass flow |
| $W_{egr}$ | [kg/s] | EGR mass flow |
| $W_{eng,in}$ | [kg/s] | Engine in mass flow |
| $W_{eng,out}$ | [kg/s] | Engine-out mass flow |
| $W_{es}$ | [kg/s] | Exhaust system mass flow |
| $W_{fuel}$ | [kg/s] | Fuel mass flow |
| $w_{k,n}$ | [kg] | Catalyst mass, segment k, layer n |
| $W_{trb}$, $W_{cmp}$ | [kg/s] | Turbine/compressor mass flow |
| $W_{urea}$ | [kg/s] | Urea mass flow |
| $x_{egr}$ | [1] | EGR fraction |
| $x_{H2O}$ | [1] | Molar ratio water to urea |
| $x_{M,urea}$ | [1] | Mass fraction urea of aqueous solution |
| $x_{urea}$ | [1] | Urea conversion |
| $y_i$ | [1] | Molar fraction of specie i |
| $z$ | [m] | Axial direction in the catalyst |
| $z^*$ | [m] | Dimensionless axial direction in the catalyst |
| $\alpha_{mix}$ | [CAD] | Mixing parameter |
| $\alpha_{SOC}$ | [CAD] | Start of combustion |
| $\alpha_{SOI}$ / $\alpha_{EOI}$ | [CAD] | Start/end of injection |

| | | |
|---|---|---|
| $\beta_i$ | [1] | Coefficient for implicit method calculations (catalyst model) |
| $\delta$ | [kg/stroke] | Injected fuel mass |
| $\delta_{pilot}$ / $\delta_{main}$ | [kg/stroke] | Pilot/main injected fuel mass |
| $\Delta_{ads/des}$ | [mole/s kg] | Reaction rate adsorption-desorption |
| $\Delta H_j$ | [J/mol] | Heat of reaction j |
| $\Delta t$ | [s] | Time step length |
| $\Delta x_n$ | [m] | Wall thickness of catalyst layer n |
| $\Delta z_k$ | [m] | Length of catalyst segment k |
| $\gamma_i$ | [1] | Specific heat value ratio of specie i |
| $\Gamma_{I,k,n}$ | [m³/s] | Mass transfer coefficient, specie i in catalyst layer n, segment k |
| $\eta_\iota$ | [1] | Internal effectiveness factor |
| $\eta_{trb}$, $\eta_{cmp}$ | [1] | Turbine/compressor efficiency |
| $\lambda$, $\lambda_{local}$ | [1] | Global/local lambda (air-fuel ratio relative to the stoichiometric air-fuel ratio) |
| $\lambda_i$ | [W/m K] | Heat conductivity, component i |
| $\nu$ | [1] | Stoichiometric coefficient/stoichiometric ratio |
| $\theta$ | [CAD] | Crank angle degree |
| $\theta_{NH3}$ | [1] | Catalyst ammonia coverage |
| $\theta_{NH3,avg}$ | [1] | Average catalyst ammonia coverage |
| $\theta_{NH3,ss}$ | [1] | Steady state catalyst ammonia coverage |
| $\rho_x$ | [kg/m³] | Density of x |
| $\tau$ | [s] | Characteristic time constant, first order method calculations |
| $\tau_{MPC}$ | [s] | Characteristic time constant, MPC |
| $\omega_{trb}$, $\omega_{cmp}$ | [rad/s] | Turbine/compressor angular speed |
| $\Omega_x$ | [g/kWh] / [1] / [ppm] | Feasible set of x |
| $\Psi$ | [1] | Compressible flow function |

| | |
|---|---|
| CAD | Crank Angle Degree |
| DPF | Diesel Particulate Filter |
| EGR | Exhaust Gas Recirculation |
| ETC | European Transient Cycle |
| ESC | European Stationary Cycle |
| LD | Legal Demand |
| MPC | Model Predictive Control |
| PM | Particulate Matter |
| SCR | Selective Catalytic Reduction |
| SQP | Sequential Quadratic Programming |
| VGT | Variable Geometry Turbine |
| WHSC | World Harmonized Stationary Cycle |
| WHTC | World Harmonized Transient Cycle |

# Contents

# 1 Introduction

During the past decade, the automotive industry has put an enormous amount of research and development into creating a cleaner diesel engine. The development has been forced by increasingly strict emissions legislation from both European and American authorities. In the 90's, Euro III emissions were achieved using higher injection pressure for low particulate emissions and retarded injection for lower $NO_x$ emissions. Euro IV emissions however, proved difficult to achieve using traditional technology. Some manufacturers introduced cooled EGR to decrease $NO_x$, others used Selective Catalytic Reduction (SCR) using urea/AdBlue as reduction agent. Using SCR, the injection timing can be advanced which gives favourable fuel economy. Engines achieving Euro V emission levels have also been demonstrated using either EGR or SCR technology. The Euro VI standard is yet to be determined; a reasonable guess is that the level will be around 0.5 g/kWh $NO_x$ and 10 mg/kWh PM. Such low levels will require even more advanced engine technology and more optimization work. Hydrocarbon (HC) and carbon monoxide (CO) are also regulated, although these emission levels are generally not difficult to achieve in diesel engines due to the high air-fuel ratio.
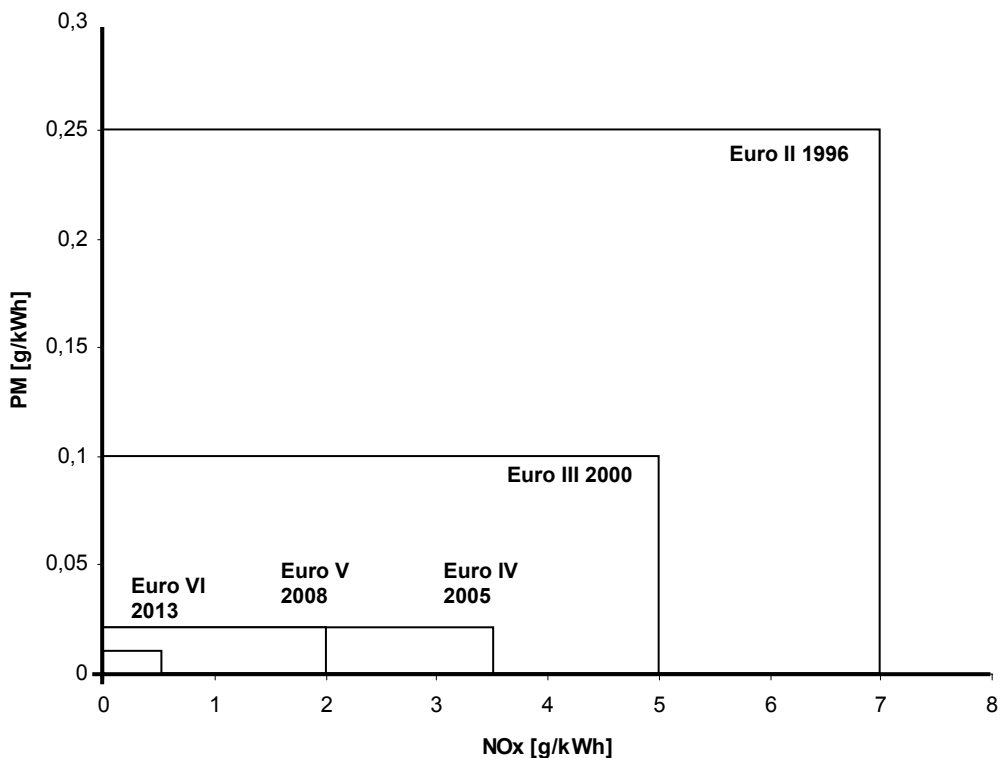


**Figure 1.1 Historical view of emission legislation for heavy truck and bus engines.**

$CO_2$ emissions are currently not regulated by legislation. In the near future it is likely that such legislation will come into effect, or possibly taxation which will increase the demand for fuel efficient engines with correspondingly low $CO_2$ emissions. Fuel efficiency has always been an important factor for heavy truck customers; despite this the efficiency of the typical heavy duty engine has not been significantly improved over the last decade because of the stringent $NO_x$/PM legislation. The trade-off between low emissions and fuel efficiency will be an even more important challenge in the close future for diesel engine developers.

## 1.1  Selective Catalytic Reduction

Selective Catalytic Reduction (SCR) of $NO_x$ using ammonia, $NH_3$ or urea, $CO(NH_2)_2$ as reduction agent has been around since the 1970's in power plants and other stationary applications. In the 1990's SCR systems for mobile applications were developed, at first for marine applications and in 2004 the first commercially available heavy truck with a urea-SCR system was launched. Urea is typically the preferred reduction agent in mobile applications because of its odour-free non-poisonous properties. Urea is sold commercially as an aqueous solution consisting of 32.5 % urea under the name AdBlue.

A urea-SCR system consists of three major building blocks:

1.  Urea dosing system

2.  Control system

3.  SCR catalyst

The urea is injected into the exhaust stream from the urea dosing system. The injection point should preferably be some distance before the catalyst to ensure proper mixing. The urea is decomposed (thermolyzed) to ammonia and isocyanic acid. The isocyanic acid is further hydrolyzed to ammonia and carbon monoxide. The ammonia reacts on the catalyst surface with NO (the DeNOx reaction) according to:

$$2NH_3 + 2NO + \frac{1}{2}O_2 \rightarrow 2N_2 + 3H_2O$$
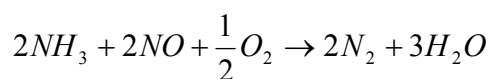
The result after the reduction is nitrogen and water only. Unfortunately, it is very difficult to reach 100 % $NO_x$ reduction, especially during transient conditions. One of the key factors for achieving high conversion is temperature. The SCR catalyst has a temperature window with a lower limit of approximately 200 ºC and a higher limit of approximately 450-500 ºC. Outside this window, the reduction capability of the catalyst is severely decreased. At low temperatures the $NO_x$ reduction is kinetically limited (due to the low temperature) and at high temperatures the DeNOx reaction rate is limited by low $NH_3$ surface coverage (the $NH_3$ desorption rate increases faster with temperature than the DeNOx reaction rate). The catalyst also has much slower dynamics compared to the engine; the catalyst typically requires several minutes before reaching chemical equilibrium compared to a few milliseconds for the diesel engine.

The equilibrium is strongly temperature dependent; Figure 1.2 shows the equilibrium mass $NH_3$ stored in a typical HD SCR catalyst as a function of temperature. It is also important to have proper control of the urea dosing to avoid ammonia slip, i.e. ammonia in the exhaust gas after the catalyst. Ammonia has a distinct unpleasant smell and is also regulated by legislation.
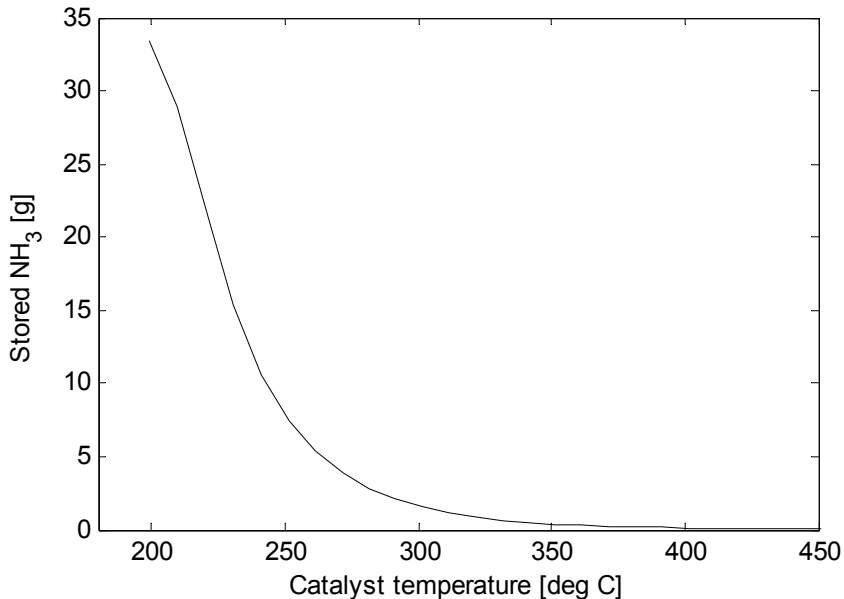


**Figure 1.2 Equilibrium stored NH$_3$. Molar flow 10 mole/s, NO fraction 500 ppm, Urea/NO stoichiometry 0.90, 30 l vanadia based SCR catalyst.**

The dominating catalyst structure used in automotive applications is the monolith, illustrated in Figure 1.3. The monolith catalyst achieves high surface area and yet a low pressure drop. Two types of monolith catalysts are commercially available. The first type is built on an inert structure, generally consisting of cordierite, $2MgO \cdot 2Al_2O_3 \cdot 5SiO_2$. The inert structure is coated with a porous material (the washcoat) which further increases the surface area. The most common washcoat material in SCR catalysts is Titanium dioxide, $TiO_2$. The washcoat is impregnated with the catalytically active elements. In the second type of monolith catalysts, the entire catalyst structure incorporates the catalytic material, i.e. no inert material is used. Different additives such as silica are used to create the monolith structure. Historically, the most common active ingredient in automotive SCR catalysts is vanadium pentoxide, $V_2O_5$ mixed with tungsten trioxide, $WO_3$. Recently catalysts based on copper/iron zeolite (Cu/Fe-ZSM5) have gained popularity due to their higher maximum operating temperature. In combined DPF/SCR systems where the SCR catalyst is placed after the DPF, the catalyst will be exposed to temperatures in excess of 600 $^o$C (during active regeneration) which will damage a vanadia based catalyst. Zeolite based catalysts on the other hand suffer from problems such as sulphur and hydrocarbon poisoning [1].

*washcoat*
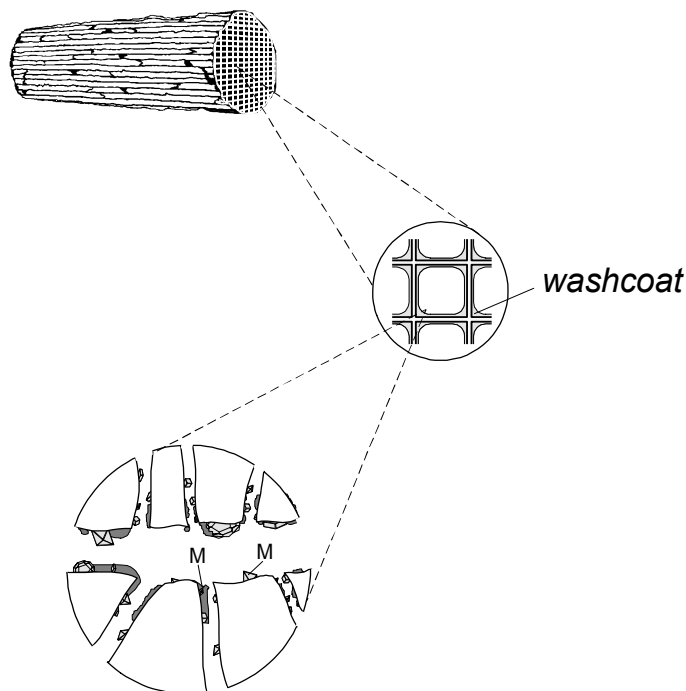
**Figure 1.3 Illustration of a typical monolith catalyst and its porous structure. M indicates active material. Reprinted with permission from Linda Hellström.**

## 1.2   Exhaust Gas Recirculation

Exhaust Gas Recirculation (EGR) has been used for decades, although the first heavy duty applications appeared on the market in 2002 as a measure to meet the US 2004 and Euro IV legislations [2]. There are two basic types of EGR systems:

1.   High pressure loop EGR: a portion of the exhaust flow is circulated to the intake manifold from the exhaust manifold (prior to the turbine). A pressure difference is needed to drive the EGR flow; this is typically achieved using for example a venturi, intake throttling or a Variable Geometry Turbocharger (VGT).

2.   Low pressure loop (long route) EGR: exhaust gas is circulated to the intake from a post turbine location. In order to avoid rapid deterioration of the compressor and charge air cooler, a Diesel Particulate Filter (DPF) is usually installed prior to the exhaust sourcing point.

In both cases, the flow is controlled by a valve and a cooler is used to decrease the temperature of the EGR gas. Numerous advantages and disadvantages exist with both concepts, although high pressure loop EGR is the most common solution today. The main advantage of using EGR is reduced $NO_x$ emissions. Four effects can explain the reduction in $NO_x$ [2,3]:

   i.   Dilution effect: adding EGR reduces the mass fraction of oxygen in the cylinder.

   ii.   Thermal effect: introducing EGR will increase the specific heat capacity of the cylinder charge.

   iii.   Chemical effect: temperature decrease due to for example dissociation of $H_2O/CO_2$, which is an endothermic reaction.

   iv.   Added mass effect: increased cylinder charge mass due to EGR results in a higher overall heat capacity of the cylinder contents.

All four effects combined result in decreased $NO_x$ emissions due to a lower flame temperature. The dilution effect, which is the most important, will also result in a decreased (global) oxygen concentration which does decrease $NO_x$ formation, but the reduced flame temperature is still the main explanation.

The first attempts using EGR on diesel engines, where a portion of the fresh air was replaced with EGR, resulted in increases in both PM emissions and fuel consumption [2]. One explanation is higher intake temperature due to insufficient cooling of the EGR. The decrease in oxygen fraction due to the dilution effect will also have a negative impact on PM emissions. A more suitable approach is to use additional EGR [3], i.e. keeping the oxygen concentration constant by increasing the total cylinder charge. Recently developed EGR engines use the additional EGR approach combined with improved fuel injection systems and do not significantly suffer from increased fuel consumption nor increased PM emissions. Using high pressure loop EGR, an increase in pumping work (which adversely affects fuel consumption) is difficult to avoid however.

## 1.3   Test Cycles

Heavy truck engines are certified in an engine test bed using certain test cycles, usually one steady state cycle and one transient test cycle. In Europe, the current (Euro V) test cycles are the European Stationary Cycle (ESC) and the European Transient Cycle (ETC) [2]. The ESC consists of a total of 13 operating points, one idle point and four load points (25-100% load) at three different speeds. The ETC is divided into three parts: urban, rural and motorway driving. Both the ESC and the ETC are characterized by relatively high load and high exhaust temperatures.

Starting from Euro VI, new test cycles are introduced; the World Harmonized Stationary Cycle (WHSC) and the World Harmonized Transient Cycle (WHTC). The WHSC has a length of 1895 s and is defined according to Table 1.1. Unlike the ESC, speed/torque is ramped between the different modes and emissions are measured continuously throughout the whole test cycle. The WHSC is hot started, preconditioned using mode 9. In general, the WHSC contains a larger portion of low speeds and low loads compared to the ESC.

The WHTC has a length of 1800 s, starting with a highly transient part (urban driving) and ending with a sequence with higher load and less transience (highway driving). Speed and load as a function of time is given in Figure 1.4. The certification procedure includes a cold and hot start WHTC run. The hot and cold start parts are separated with a hot soak period when the engine is turned off. Emissions are calculated by weighting the two parts together. Compared to the ETC, the load is generally lower, particularly during the urban driving part. Also, the number of idle and motoring sequences is substantially larger. The result is lower exhaust temperature; achieving high $NO_x$ conversion over the SCR catalyst is therefore more challenging.

The most problematic part is the first ~400 s where the exhaust temperature for a typical heavy duty engine is 200 °C or less in both the hot and cold start cases.

**Table 1.1 Definition of the WHSC.**

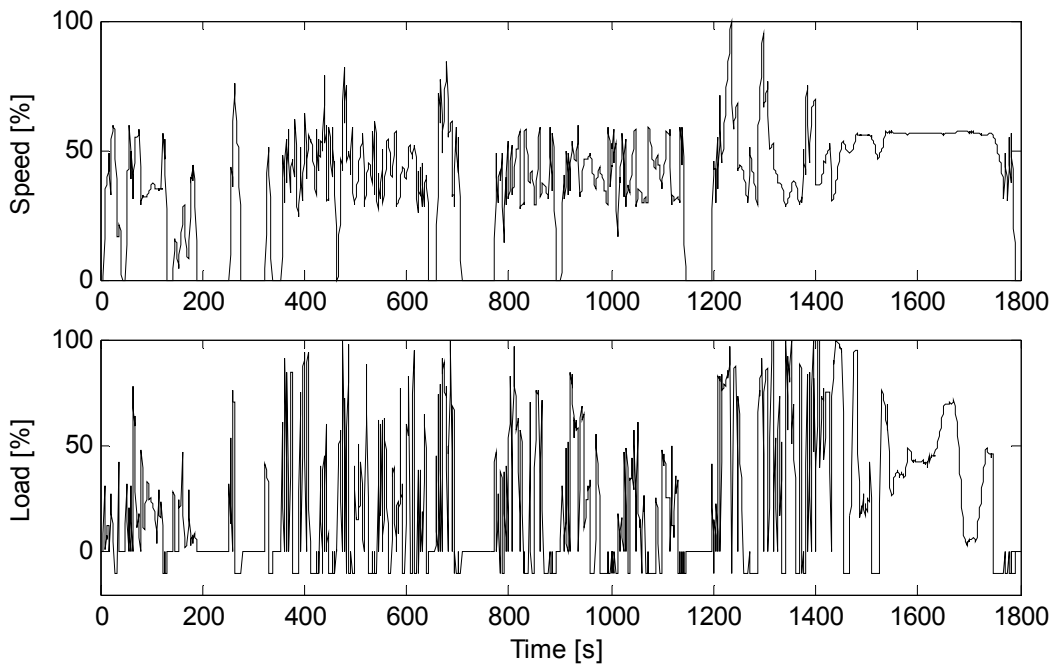| Mode | Speed | Torque | Time |
|------|-------|--------|------|
| 0 | Motoring | - | - |
| 1 | 0 | 0 | 210 |
| 2 | 55 | 100 | 50 |
| 3 | 55 | 25 | 250 |
| 4 | 55 | 70 | 75 |
| 5 | 35 | 100 | 50 |
| 6 | 25 | 25 | 200 |
| 7 | 45 | 70 | 75 |
| 8 | 45 | 25 | 150 |
| 9 | 55 | 50 | 125 |
| 10 | 75 | 100 | 50 |
| 11 | 35 | 50 | 200 |
| 12 | 35 | 25 | 250 |
| 13 | 0 | 0 | 210 |



**Figure 1.4 Speed and load profile of the WHTC.**

## 1.4 The Optimization Problem

To achieve emission levels corresponding to Euro VI or beyond while maintaining good fuel economy, it is important that the engine and its aftertreatment system is optimized using a complete system approach. The aftertreatment system usually consists of either an oxidation catalyst, a DPF or a SCR catalyst or combinations thereof. In the work presented in this thesis, SCR only is considered. Optimizing the complete system is not a trivial task because of the large number of variables which control emissions and fuel consumption in the complex diesel engines of today. Assuming that the engine incorporates a common rail fuel injection system, an EGR system aided by a Variable Geometry Turbocharger (VGT) and a urea SCR system, the following variables must be optimized in each operating point:

- Injection timing
- Injection pressure
- Pilot/post injections
- EGR valve position
- VGT actuator position
- Urea dosing

Clearly, this requires substantial time in the engine test bed if all combinations of these variables are to be tested. In addition, because of the slow dynamics of the SCR catalyst, the optimization problem is time dependent making it a complex task. Factors such as urea versus diesel fuel costs and driving conditions can also affect the optimal calibration of the complete engine/aftertreatment system.

A novel approach to solve these problems is to use model based optimization and control.

## 1.5 Objective

The objective of the work presented in the thesis is to develop methods for optimizing fuel consumption and emissions of the complete system diesel engine plus SCR catalyst.

## 1.6 Method

A modelling approach is used to solve the problem. The first step involves developing computationally efficient models of the diesel engine, the exhaust system and the SCR catalyst. The models should preferably be of such simplicity that they can be executed in real time in the engine control system or millions of times in a short time span in the process of offline optimization.

In the second step, the models are applied for characterization and optimization of the system. Operating sequences which are critical to the overall performance of the system are identified. Finally, the optimization problem is formulated and solved aiming at minimizing fuel consumption/$CO_2$ emissions while maintaining emissions at Euro VI levels.

# 2   Engine Model

In this chapter, the engine model is presented. The model consists of two parts, a combustion model and a gas exchange model. The modelled engine is an inline six cylinder experimental engine using cooled EGR. The engine is equipped with a variable geometry turbocharger (VGT) and a common rail fuel injection system. A large number of variables are introduced in this chapter which are all defined in the Notation and Acronyms Section. In all models presented in this thesis, $NO_x$ is considered to consist of NO only; typically less than 10% of the $NO_x$ engine out is $NO_2$.

## 2.1   Combustion Model

The combustion model consists of a predictive heat release/combustion model and a $NO_x$ formation model. First, a short literature survey is given.

### 2.1.1   Literature Survey

The conceptual model for diesel combustion presented by Dec [4] is the base for most of the recent work in the area. The model states that the diesel combustion is divided into two parts; the first step involves a fuel rich premixed combustion where soot is formed but the $NO_x$ formation is limited. More air is entrained in the spray, and the second part of the combustion, mixing controlled (diffusion) combustion, is formed at close to stoichiometric conditions. $NO_x$ is formed on the lean side of the diffusive layer.

Chmela et al. [5] discuss zero dimensional prediction of heat release rate during diffusion combustion. The model is based on the assumption that the heat release rate is proportional to the fuel energy available for combustion. It is also identified that the combustion is mainly turbulence controlled, i.e. the reaction rate is limited by the air-fuel mixing. The mixing process is identified to be most strongly influenced by the kinetic energy of the fuel spray. The result is a zero dimensional mixing controlled combustion model which shows good agreement with measurements.

The work is extended by Chmela et al. [6] with models for ignition delay and premixed combustion. A transition function is introduced to describe how injected fuel is divided between the premixed and diffusion combustion parts. The diffusion combustion model from [5] is slightly revised using a linear rather than an exponential dependency on the turbulence term. Pirker et al. [7] present a further evolution of the model. Ignition delay is modelled as a combination of air-fuel mixing rate and the chemical reaction rate. The diffusion combustion model is modified to treat the combustion as two sequential phases; prior to and after the end of fuel injection.

Egnell [8,9,10] uses a simplified form of the Chmela predictive heat release model [5]. The influence of kinetic spray energy is accounted for using empirically determined proportionality factors between fuel rate and heat release rate. Modelling NO formation is discussed thoroughly and a multi zone model is developed. The burned zone temperatures are calculated using a Gibbs free energy minimization iteration and $NO_x$ formation is given by the original/extended Zeldovich equilibrium approach. A full kinetic approach is also presented where the concentration of all species (not only $NO_x$) is considered time dependent.

Andersson [11,12] presents a modified version of Chmelas' diffusion combustion model [6]. Chmela defines the characteristic length as the cubic root of the current cylinder volume while Andersson uses a measure on the mean distance between oxygen molecules. Another difference is the addition of swirl generated kinetic energy. The spray generated turbulence is considered to decay exponentially after fuel injection has ended. A computationally efficient multi zone $NO_x$ formation model is also presented. The model calculates burned zone temperatures using tabulated data to calculate the difference between perfect and real combustion. NOx formation is given by the Zeldovich mechanism.

Siewert [13] presents a more detailed fuel injection and spray model compared to the previous references. Ignition delay is modelled as a combination of evaporation and reaction time. Premixed and diffusion combustion is modelled using empirical expressions. Simplified models for $NO_x$ and soot formation are also presented. Good agreement is shown with measurement data, although the overly simplified combustion and $NO_x$ formation models are not found to be useful in the model developed in the thesis work.

### 2.1.2    Basic Assumptions

The model is based on the zero dimensional models presented by Egnell [8,9,10] and Andersson [11,12]. The main focus of the work presented in this chapter is improving computational efficiency while maintaining good agreement with measurements. The model is zero dimensional and uses two zones. Egnell [10] concludes that reasonable accuracy can still be achieved using two zones compared to multi zones (by altering the local lambda). More significantly, the simulation time is reduced with a factor ~10 with a two zone approach. The combustion chamber contents are divided into one unburned zone which consists of air and EGR, and one burned zone containing the burned results of injected fuel and previous unburned zone contents (Figure 2.1).
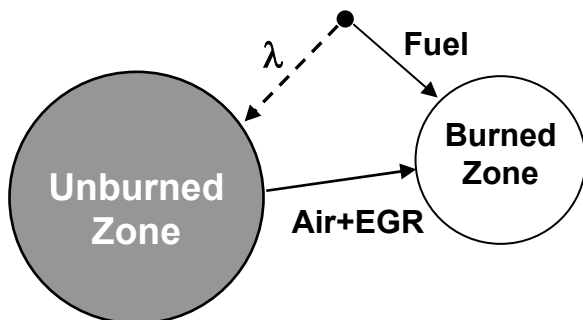


**Figure 2.1 Illustration of the two zone concept.**

A number of assumptions analogously with Egnell [10] have been made in the modelling process:

- The cylinder content can be described as an ideal gas.
- All combustion takes place at the same local air-fuel equivalence ratio.
- There are no pressure gradients inside the cylinder.
- No air entrainment occurs in the burned zone.
- The zones are compressed isentropically.
- All injected fuel is fully burned.
- Radiative heat losses originate from the flame only.
- $NO_x$ is formed in the burned zone.
- All $NO_x$ content in the recirculated exhaust gas is neglected.
- All released energy originates from injected fuel.

### 2.1.3 Predictive Heat Release Model

The heat release model is of the predictive type, i.e. in-cylinder pressure measurements are not needed as inputs.
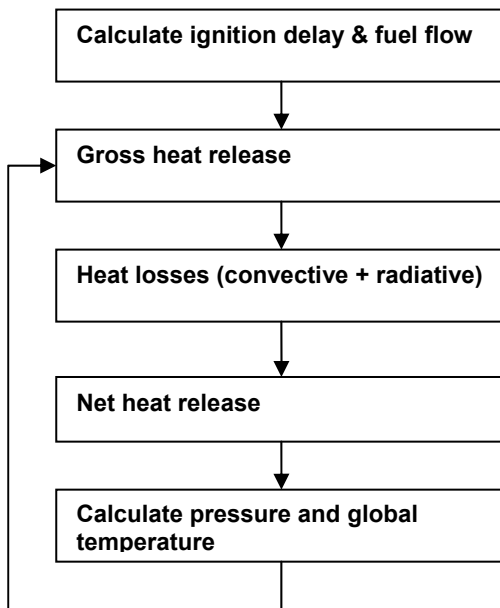


**Figure 2.2 Flowchart of the heat release loop.**

A flowchart of the predictive heat release loop is shown in Figure 2.2. The algorithm will now be described in more detail. First, the ignition delay is calculated using the following expression:

$$\alpha_{SOC} - \alpha_{SOI} = g_{ID,1}\left(N_{eng}\right) \cdot g_{ID,2}\left(\delta_{pilot}\right) \cdot c_{O_2}{}^{K_1} \cdot p_{rail}{}^{K_2} \cdot e^{K_3\left(\frac{1}{R \cdot T_{SOI}}\right)} \tag{2.1}$$

where $K_x$ are constant parameters tuned to fit measured ignition delay. The correlation is basically the inverse of a second order reaction rate.

The polynomial functions $g_{ID,1}$ and $g_{ID,2}$ compensate for deviations at low engine speeds and pilot injections respectively. Assuming a top-hat profile of the needle lift, fuel mass flow is constant during the injection duration and is usually considered proportional to the square root of the pressure differential. Such a simple model will not provide good agreement with measurements however, especially at low injected fuel mass. Instead, an empirically determined modified version of the square root correlation is used:

$$W_{fuel} = \frac{\delta}{K_{f,1} + \dfrac{\delta}{K_{f,2} + K_{f,3}\sqrt{p_{rail}}}}$$
(2.2)

where $\delta$ is the injected fuel mass, $p_{rail}$ is the fuel injection pressure and $K_{f,x}$ are constants. Using the calculated fuel mass flow, the injected fuel energy at a crank angle $\theta$ is given by:

$$Q_{fuel,inj} = Q_{LHV} \int_{\alpha_{SOI}}^{\theta} W_{fuel}(\theta)\,d\theta$$
(2.3)

where $Q_{LHV}$ is the lower heating value of the fuel and $\alpha_{SOI}$ the start of injection. The total energy released during the premixed combustion is calculated according to:

$$Q_{premix,tot} = \frac{dQ_{fuel,inj}}{d\theta} \cdot \left( \min(\alpha_{EOI}, \alpha_{SOC} - \alpha_{mix}) - \alpha_{SOI} \right)$$
(2.4)

where $\alpha_{mix}$ is a fuel mixing parameter. Two different cases exist, depending on the relation between EOI and SOC, as illustrated in Figure 2.3. In the second case where SOC occurs before EOI, the mixing parameter is required to get an accurate balance between premixed and diffusion combustion.
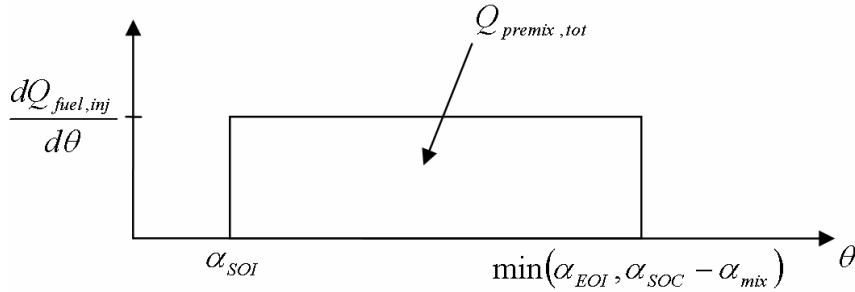


**Figure 2.3 Illustration of total energy released during premixed combustion.**

The mixing parameter is given by a gray box expression (derived in paper V):

$$\alpha_{mix} = K_{mix,1} \cdot \frac{1}{u_f^{K_{mix,2}} \sqrt{\rho_g}\left(1 - \dfrac{x_{egr}}{\lambda}\right)} \cdot 6 \cdot N_{eng}$$
(2.5)

where $K_{mix,1}$ and $K_{mix,2}$ are constants. A similar approach is used by Pirker et al. [7] where a constant determines the fraction of the injected fuel amount injected during the ignition delay dedicated to premixed combustion.

The maximum heat release rate of the premixed combustion is calculated according to:

$$\left( \frac{dQ_{g,premix}}{d\theta} \right)_{max} = r_{premix,max} \cdot Q_{premix,tot} \tag{2.6}$$

where

$$r_{premix,max} = K_{pre,1} \cdot c_{O_2,SOC}{}^{K_{pre,2}} \cdot e^{-\frac{K_{pre,3}}{T_{SOC}}} \cdot N_{eng}{}^{K_{pre,4}} \tag{2.7}$$

The premix heat release rate is then given by:

$$\frac{dQ_{g,premix}}{d\theta} = \left( \frac{dQ_{g,premix}}{d\theta} \right)_{max} + g_{pre1} \left( \theta - g_{pre2} \right)^2 \tag{2.8}$$

The parameters $g_{pre1}$ and $g_{pre2}$ are calculated to fit the integrated heat release rate to total released energy. Siewert [13] applies a similar concept for calculating premixed heat release rate, although the maximum heat release rate is an entirely empirical expression.

Diffusion combustion heat release rate is calculated according to:

$$\frac{dQ_{g,diff}}{dt} = C_{diff} \left( Q_{fuel,inj,diff} - Q_{g,diff} \right) \tag{2.9}$$

where

$$Q_{fuel,inj,diff} = Q_{fuel,inj} - Q_{premix,tot} \tag{2.10}$$

and

$$C_{diff} = c_{O_2}{}^{1/3} \sqrt{ K_{spray} \cdot p_{rail} \cdot y_{O_2} \cdot e^{-K_{fade} \cdot t_{AEOI}} + K_{swirl} \cdot N_{eng}^2 } \tag{2.11}$$

This expression is a lumped parameter version of the diffusion combustion model by Andersson et al. [11]. The constant parameters $K_{spray}$, $K_{fade}$ and $K_{swirl}$ are tuned to fit measured heat release rates. The resulting total heat release rate is given by:

$$\frac{dQ_g}{d\theta} = \frac{dQ_{g,premix}}{d\theta} + \frac{dQ_{g,diff}}{d\theta} \tag{2.12}$$

A typical heat release rate curve as given by the model is shown in Figure 2.4. The figure also illustrates the three phases of the heat release (SOI=-4 CAD in this case).
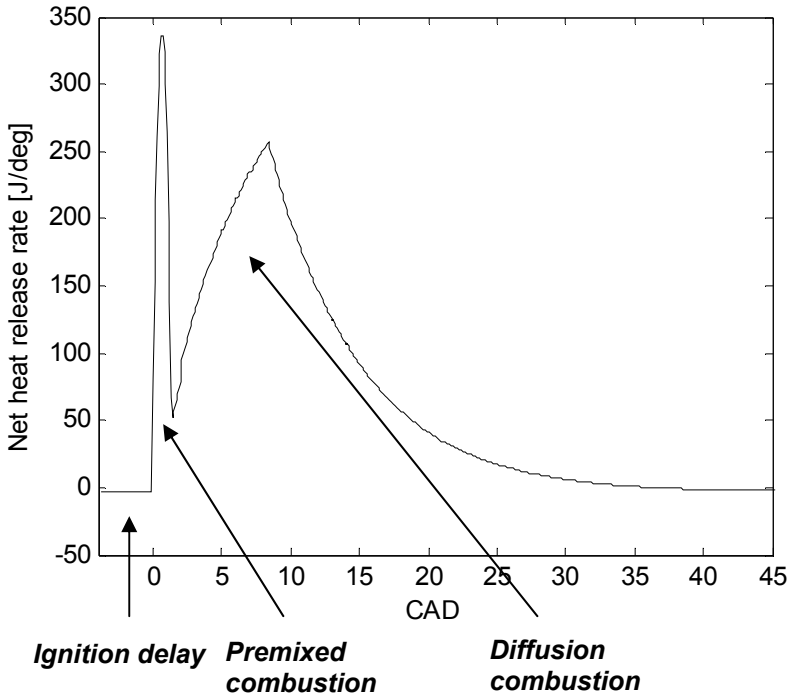
**Figure 2.4 Illustration of the three phases of diesel combustion.**

Convective heat losses using the cylinder temperature from the previous crank angle step are given by:

$$\frac{dQ_{ht,conv}}{dt} = A \cdot h_c \cdot (T - T_{wall}) \tag{2.13}$$

The area $A$ is calculated using the geometric properties of the engine. The gas temperature used is the global in-cylinder gas temperature $T$ (from the previous crank angle step). The wall temperature $T_{wall}$ is fixed at 450 K and $h_c$ is calculated using the Woschni expression [14] as:

$$h_c = C_{wo} B^{-0.2} p^{0.8} u^{0.8} T^{-0.55} \tag{2.14}$$

where $B$ is the cylinder bore, $p$ the cylinder pressure and $C_{wo}$ is an empirically determined constant. The average gas cylinder velocity is given by [14]:

$$u = K_{w,1} S_p + K_{w,2} \frac{V_{disp}}{n_{cyl} R} (p - p_{motored}) \tag{2.15}$$

where $S_p$ is the mean piston speed, $V_{disp}$ is the displaced volume, $n_{cyl}$ is the molar number of the cylinder charge and $p_{motored}$ is the motored cylinder pressure.

The flame radiative heat losses are calculated using the adiabatic flame temperature $T_{flame,ad}$ (from the previous crank angle step):

$$\frac{dQ_{ht,rad}}{dt} = \dot{n}_{flame} C_{rad} T_{flame,ad}{}^4 \tag{2.16}$$

The flame temperature is substantially higher than the wall temperature, therefore Equation (2.16) is written in a simplified form with $T_{wall}$ omitted. The factor $C_{rad}$ is not a strictly physical parameter, it is used in the final step of the combustion model tuning to fit simulated to measured $NO_x$.

Combining the equations, the net heat release is:

$$\frac{dQ_n}{d\theta} = \frac{dQ_g}{d\theta} - \frac{dQ_{ht,conv}}{d\theta} - \frac{dQ_{ht,rad}}{d\theta} \tag{2.17}$$

Finally, the pressure is calculated by rearranging the first law of thermodynamics (assuming that the gas composition is constant between two crank angle steps):

$$\frac{dp}{d\theta} = \left( \frac{dQ_n}{d\theta} - \frac{\gamma_{cyl}}{\gamma_{cyl} - 1} p \frac{dV}{d\theta} \right) \left( \frac{\gamma_{cyl} - 1}{V} \right) \tag{2.18}$$

where the ratio of specific heats of the cylinder contents, $\gamma_{cyl}$, is calculated using thermodynamic curve fit coefficients [15]. The global combustion temperature is now given using the ideal gas law.

This sequence of calculations is performed with a fixed crank angle interval. Typically the heat release loop uses a step of 0.1-0.2 CAD in order to capture the rapid changes during the early parts of the heat release.

Exhaust manifold temperature can be estimated fairly accurately using the simulated temperature and pressure at exhaust valve opening, $T_{evo}$ and $p_{evo}$. A substantial temperature drop will occur from the gas temperature at exhaust valve opening to the exhaust manifold. A simple model is fitted to experimental data with good accuracy:

$$T_{em} = T_{evo} \cdot \left( \frac{p_{em}}{p_{evo}} \right)^{\frac{\gamma_{em} - 1}{\gamma_{em}}} \tag{2.19}$$

Note that the exhaust flow from inside the cylinder to the exhaust manifold is not a polytropic process; Equation (2.19) should be considered a black box expression. The constant $\gamma_{em}$, is tuned to fit the model to experimental data.

### 2.1.4 Burned Zone / NO$_x$ Formation Model

Calculations of burned zone temperature and NO$_x$ formation are executed in a separate loop. This loop is executed more sparsely than the heat release loop in order to save computational time.

In the model presented by Egnell [8], an iteration loop based on the minimization of Gibbs free energy is performed in each crank angle step. The iteration determines the gas composition and the burned zone temperature. This type of model requires too much computational power in order to be used for engine control and transient simulation applications. A simplified method of calculating burned zone temperature in a multi-zone model is presented by Andersson et al. [11,12]. A two zone approach of this method has been implemented in this model. Locally stoichiometric combustion is assumed ($\lambda_{local} = 1$) and no air entrainment in the burned zone occurs.
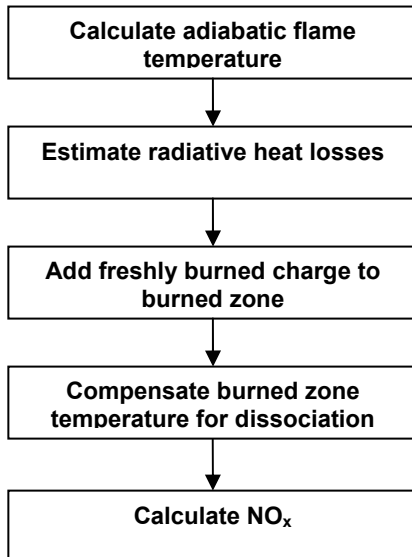


Figure 2.5 Flow chart of the burned zone/NO$_x$ formation loop.

The algorithm for updating the burned zone and calculating NO$_x$ formation is presented as a flowchart in Figure 2.5. First the adiabatic flame temperature is calculated using enthalpy balance between an unburned mass element and a perfectly combusted burned mass element. The enthalpy of the unburned gas mixture is given by:

$$h_{unburnt} = (1 - x_{egr}) \cdot h_{air} + x_{egr} \cdot h_{egr} + h_{fuel} \tag{2.20}$$

where

$$h_{egr} = \frac{\lambda - 1}{\lambda} \cdot h_{air} + \frac{1}{\lambda} \cdot h_{burnt, \lambda=1} \tag{2.21}$$

The enthalpies $h_{air}$, $h_{fuel}$ and $h_{burnt,\lambda=1}$ are calculated using linear enthalpy approximations:

$$h_x = K_{h_x 1} + K_{h_x 2} \cdot T \tag{2.22}$$

Given limited temperature ranges, the enthalpy calculations in [15] can be accurately linearized. The burned zone will consist of $N_2$, $CO_2$ and $H_2O$ only at all times due to the stoichiometric assumption. The adiabatic flame temperature is therefore given directly by:

$$T_{flame,ad} = \frac{h_{unburnt} - K_{h_{burnt,\lambda=1}1}}{K_{h_{burnt,\lambda=1}2}} \qquad (2.23)$$

A new flame temperature which is compensated for radiative heat losses can be calculated according to:

$$T_{flame,ht} = T_{flame,ad} - \frac{C_{rad}T_{flame,ad}^{\,4}}{c_{p,burnt,\lambda=1}} \qquad (2.24)$$

Note that the adiabatic flame temperature is never achieved in reality, this is just a number used in the simplified combustion model. The freshly burned mass element is then added to the burned zone. Using the energy balance and assuming that the specific heats are equal, the burned zone temperature is given by:

$$T_{burn,perf}(\theta) = \frac{T_{exp}m_{burn}(\theta - \Delta\theta) + T_{flame,ht}m_{flame}(\theta)}{m_{burn}(\theta)} \qquad (2.25)$$

where $T_{exp}$ is the isentropically expanded temperature from the previous crank angle step, $m_{burn}$ denotes the mass in the burned zone and $m_{flame}=m_{burn}(\theta)-m_{burn}(\theta-\Delta\theta)$ is the mass of the freshly burned element (flame).

In order to compensate for dissociation, tabulated data is used. A simplified method is used where the combustion is considered to be perfect and then a table describes the temperature drop which would occur if the combustion products ($CO_2$, $H_2O$ and $N_2$) dissociate adiabatically to CO, $CO_2$, $H_2$, H, OH, O, $O_2$, NO, $H_2O$, $N_2$ and N. The method is illustrated in Figure 2.6. It is a function of pressure, temperature and local air-fuel equivalence ratio. The table is generated using a Gibbs free energy minimization approach analogously to Egnell [8]. The compensated burned zone temperature is given by:

$$T_{burn} = T_{burn,perf} - f_{eq}\left(p, T_{burn,perf}, \lambda_{local}\right) \qquad (2.26)$$
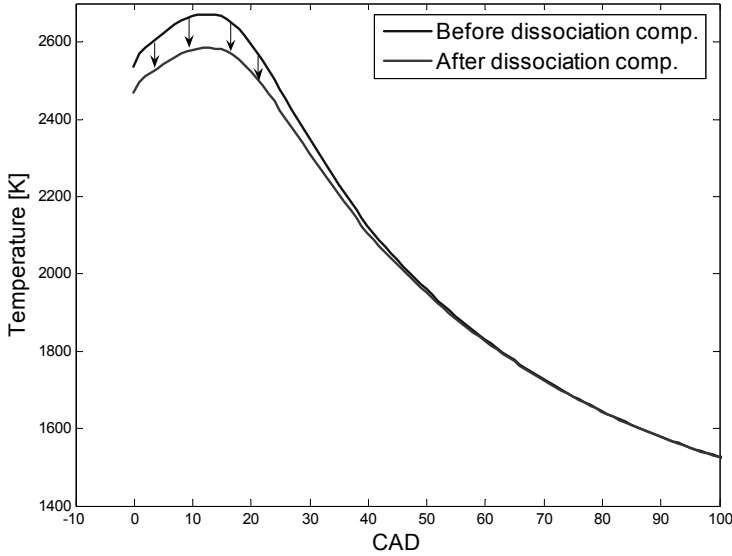
**Figure 2.6 Typical burned zone temperature before and after dissociation compensation.**

The $NO_x$ formation is modelled using the (original) Zeldovich mechanism equilibrium approach [14]. Egnell [10] has shown that both the original and the extended Zeldovich mechanisms can provide good agreement with measurements (by tuning the local lambda). In the model presented in this thesis, local lambda is fixed. Instead, the radiative heat losses are tuned to fit simulated to measured $NO_x$. The (original) Zeldovich mechanism includes the following two reactions:

$$O + N_2 \leftrightarrow NO + N \tag{2.27}$$

$$N + O_2 \leftrightarrow NO + O \tag{2.28}$$

The equilibrium approach assumes that the residence time in the flame is short; therefore the $NO_x$ formation takes place in the (post flame) burned zone only. This allows for a useful simplification; equilibrium concentrations are used for all species except for $NO_x$. Also assuming that the atomic nitrogen concentration is low and slowly varying, i.e.:

$$\frac{dc_N}{dt} = 0 \tag{2.29}$$

the following expression is derived:

$$\frac{dc_{NO}}{dt} = \frac{2r_1\left(1 - \left(c_{NO} / c_{NO,eq}\right)^2\right)}{1 + \left(c_{NO} / c_{NO,eq}\right)r_1 / r_2} \tag{2.30}$$

where

$$r_1 = k_1^{+} c_{O,eq} c_{N_2,eq} \tag{2.31}$$

$$r_2 = k_2^- c_{NO,eq} c_{O,eq} \qquad\qquad (2.32)$$

denotes the forward/backward reaction rates of Equations (2.27) and (2.28).

The equilibrium oxygen and nitrogen concentrations in the burned zone are given by look-up tables. This results in faster calculations and eliminates the need to know the exact gas composition of the burned zone as in previous models [10].

To get improved performance at lower loads, a correction factor analogously to Andersson et al. [11] is applied at $NO_x$ levels below 200 ppm:

$$y_{NOx,corr} = K_{NOx,corr,1} \cdot y_{NOx,uncorr}^{K_{NOx,corr,2}} \qquad\qquad (2.33)$$

where $K_{NOx,corr,x}$ are constant parameters.

### 2.1.5 Torque Model

Brake Mean Effective Pressure (BMEP) is given by:

$$BMEP = IMEP\text{-}PMEP\text{-}FMEP \qquad\qquad (2.34)$$

Pumping Mean Effective Pressure (*PMEP*) is estimated using inlet and exhaust manifold pressures. The Friction Mean Effective Pressure (*FMEP*) is divided into two parts:

$$FMEP = FMEP_{fric} + FMEP_{hpp} \qquad\qquad (2.35)$$

The first term describes the friction related to the moving parts of the engine and also auxiliary units such as the engine coolant pump and fan. $FMEP_{fric}$ typically has a second order relation to engine speed, $N_{eng}$. A black box correction factor is added to the second order polynomial to get better agreement at high loads:

$$FMEP_{fric} = \left( k_{F,1} + k_{F,2} \cdot N_{eng} + k_{F,3} \cdot N_{eng}^{\;2} \right) \cdot \left( 1 + \delta_{main}^{\;k_{F,4}} \right) \qquad\qquad (2.36)$$

where $k_{F,x}$ are empirically determined constant parameters and $\delta_{main}$ is the (main) injected fuel mass. The second part of *FMEP* describes losses in the high pressure fuel pump:

$$FMEP_{hpp} = k_{F,5} \cdot p_{rail}^{\;k_{F,6}} \cdot \delta_{main}^{\;k_{F,7}} \cdot \left( 1 + k_{F,8} \cdot N_{eng}^{\;k_{F,9}} \right) \qquad\qquad (2.37)$$

Using the calculated value of BMEP, torque is given by:

$$M = \frac{BMEP \cdot N_{cyl} \cdot V_{disp}}{4 \cdot \pi} \qquad\qquad (2.38)$$

where $N_{cyl}$ is the number of cylinders.

### 2.1.6 Computational Efficiency

Simulation time (using uncompiled Simulink code) for one cycle is approximately 8 ms on a 2.67 GHz CPU. This can be compared to a simulation time of several minutes for the HRNOx model [10], and ~1 s for the model presented by Andersson [12].

## 2.2 Gas Exchange Model

The gas exchange model uses a simple filling and emptying quasi steady concept. It is previously described by the author in reference [16]. The model is schematically depicted in Figure 2.7.
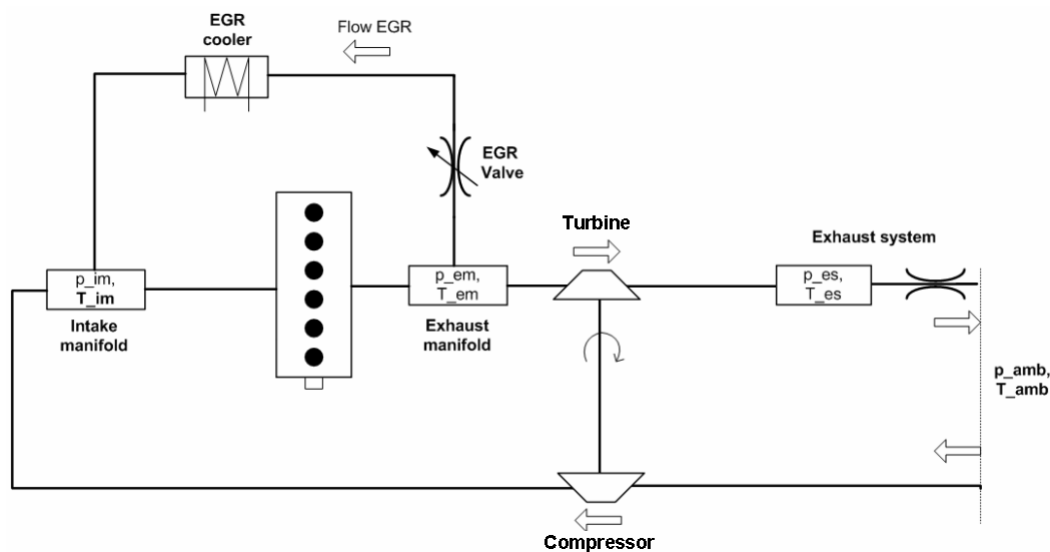


**Figure 2.7 Schematic description of the gas exchange model.**

All gas compositions are assumed to be constant, i.e. constant values for the specific heats are used. The intake manifold temperature is measured and is used as an input to the model. The reason is that it is difficult to model the charge air and EGR temperatures. Factors such as fouling of the coolers and wind conditions will affect these temperatures in onboard applications. In the laboratory using the modelled engine however, the intake manifold temperature varies in a very small range, typically 295-315 K. Using a constant value of 304 K is a good approximation [17]. The model is implemented in Simulink for optimum performance and uses a fixed time step length of 10 ms. If longer steps are used, stability problems will occur.

The different sub models will be presented following the air/exhaust path through the engine, starting from the intake side.

### 2.2.1 Compressor

The mass flow and efficiency of the compressor is calculated using look-up tables:

$$W_{cmp} = W_{cmp}\left(\frac{p_{im}}{p_{amb}}, \omega_{trb}\right)$$ (2.39)

$$\eta_{cmp} = \eta_{cmp}\left(\frac{p_{im}}{p_{amb}}, \omega_{trb}\right)$$ (2.40)

The look-up tables are based on steady state measurements of the turbocharger. The torque is given by:

$$M_{cmp} = \frac{W_{cmp} c_{p,air} T_{amb}}{\eta_{cmp} \omega_{trb}} \cdot \left(\left(\frac{p_{im}}{p_{amb}}\right)^{\frac{\gamma_{air}-1}{\gamma_{air}}} - 1\right)$$ (2.41)

$T_{amb}$ and $p_{amb}$ are the ambient temperature and pressure.

### 2.2.2 Intake and Exhaust Manifold

The intake manifold is described as a control volume (an open system of constant volume). By neglecting heat transfer and the time dependency of the temperature, the following expression is achieved by differentiating the ideal gas law:

$$\dot{p}_{im} = \frac{R_{air}}{V_{im}} \cdot T_{im}(W_{cmp} + W_{egr} - W_{eng,in})$$ (2.42)

The exhaust manifold is modelled analogously to the intake manifold:

$$\dot{p}_{em} = \frac{R_{exh}}{V_{em}} T_{em}(W_{eng,out} - W_{egr} - W_{trb})$$ (2.43)

The mass flow in to the cylinder is given by:

$$W_{eng,in} = \eta_{vol} \frac{N_{eng} p_{im} N_{cyl} V_{disp}}{2 \cdot R_{air} T_{im}}$$ (2.44)

where the volumetric efficiency $\eta_{vol}$ is a constant. The mass flow out of the cylinder is calculated according to:

$$W_{eng,out} = W_{eng,in} + \frac{\delta \cdot N_{eng} \cdot N_{cyl}}{2 \cdot 60}$$ (2.45)

### *2.2.3 EGR System*

The EGR flow is modelled using the expression for choked flow through a restriction, described by Heywood [14]:

$$W_{egr} = A_{egr} \cdot \frac{p_{em}}{\sqrt{T_{em}R_{exh}}} \cdot \psi\left(\frac{p_{im}}{p_{em}}, \gamma_{exh}\right) \tag{2.46}$$

where

$$\psi\left(\frac{p_{im}}{p_{em}}, \gamma_{exh}\right) = \begin{cases} \sqrt{\frac{2\gamma_{exh}}{\gamma_{exh}-1}\left(\left(\frac{p_{im}}{p_{em}}\right)^{\frac{2}{\gamma_{exh}}} - \left(\frac{p_{im}}{p_{em}}\right)^{\frac{\gamma_{exh}+1}{\gamma_{exh}}}\right)} & \text{if } \frac{p_{im}}{p_{em}} \geq \left(\frac{2}{\gamma_{exh}+1}\right)^{\frac{\gamma_{exh}}{\gamma_{exh}-1}} \\ \\ \sqrt{\gamma_{exh}\left(\frac{2}{\gamma_{exh}+1}\right)^{\frac{\gamma_{exh}+1}{\gamma_{exh}-1}}} & \text{if } \frac{p_{im}}{p_{em}} < \left(\frac{2}{\gamma_{exh}+1}\right)^{\frac{\gamma_{exh}}{\gamma_{exh}-1}} \end{cases} \tag{2.47}$$

$A_{egr}$ is the effective flow area of the EGR valve, a function of the valve control signal $u_{egr}$ (using a look-up table):

$$A_{egr} = A_{egr}\left(u_{egr}\right) \tag{2.48}$$

### *2.2.4 Turbine*

The mass flow and efficiency of the turbine are also calculated using look-up tables:

$$W_{trb} = W_{trb}\left(\frac{p_{em}}{p_{es}}, \omega_{trb}, u_{vgt}\right) \tag{2.49}$$

$$\eta_{trb} = \eta_{trb}\left(\frac{p_{em}}{p_{es}}, \omega_{trb}, u_{vgt}\right) \tag{2.50}$$

$u_{vgt}$ is the control signal of the variable geometry turbocharger (VGT). The influence of pulsating exhaust flow is neglected in the model; therefore the data in the turbine look-up tables are tuned to fit engine measurements. The torque and temperature after the turbine are given by:

$$M_{trb} = \frac{\eta_{trb}W_{trb}c_{p,exh}T_{em}}{\omega_{trb}} \cdot \left(1 - \left(\frac{p_{em}}{p_{es}}\right)^{\frac{1-\gamma_{exh}}{\gamma_{exh}}}\right) \tag{2.51}$$

$$T_{trb} = \left( 1 + \eta_{trb} \left( \left( \frac{p_{em}}{p_{es}} \right)^{\frac{1-\gamma_{exh}}{\gamma_{exh}}} - 1 \right) \right) \cdot T_{em} \tag{2.52}$$

The turbine speed derivative is calculated using:

$$\dot{\omega}_{trb} = \frac{M_{trb} - M_{cmp}}{J_{trb}} \tag{2.53}$$

where $J_{trb}$ is the moment of inertia of the turbocharger.

### 2.2.5 Exhaust System

The exhaust system is modelled using a control volume (analogously to the intake and exhaust manifold):

$$\dot{p}_{es} = \frac{R_{exh}}{V_{es}} T_{trb} (W_{trb} - W_{es}) \tag{2.54}$$

A quadratic restriction describes the exhaust mass flow:

$$W_{es} = \sqrt{\frac{p_{es}}{K_{es} R_{exh} T_{trb}} (p_{es} - p_{amb})} \tag{2.55}$$

where $K_{es}$ is the restriction constant.

## 2.3   Complete Engine Model

The combustion model is combined with the gas exchange model to form a complete engine model. The model structure is illustrated in Figure 2.8.
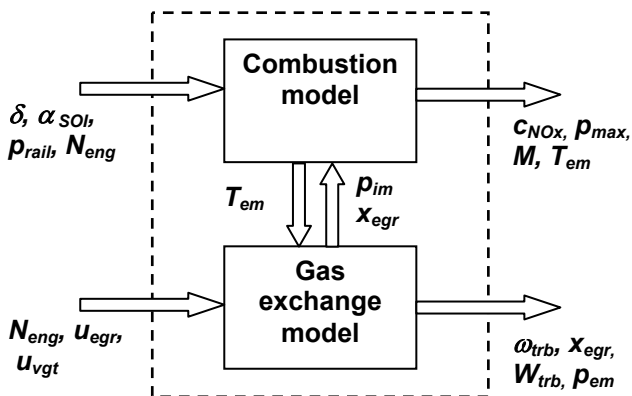


**Figure 2.8 Inputs and outputs of the complete engine model.**

The inputs are engine speed, injected fuel mass, injection timing, rail pressure, EGR valve position and VGT actuator position i.e. the typical engine control parameters available in the engine control system. A large number of output signals are possible. Typical outputs are $NO_x$ concentration, peak cylinder pressure, torque, exhaust temperature, turbine speed, EGR rate and exhaust mass flow.

The combustion model uses a 10Hz sampling time in the complete model, i.e. the combustion model is executed 10 times per second. Calculation speed for the complete model is faster than 10 times real time using uncompiled Simulink code on a 2.67GHz PC.

### 2.3.1   Control System

A simplified engine control system is added, calculating injected fuel, VGT and EGR actuator signals depending on desired versus actual torque, desired EGR rate and injection timing, illustrated in Figure 2.9. In steady state mode, the control signals are given from look up tables. In transient mode, the VGT actuator is set for maximum turbine efficiency based on the exhaust mass flow and the EGR valve is fixed to 20% of the maximum effective flow area, while the injected fuel mass is smoke limited (lambda >1.30). No feedback of the EGR rate is used; therefore, the agreement between reference and actual EGR rate during rapid transients is inadequate. A more advanced control system is beyond the scope of this thesis however. The simplified control system is used in paper IV; in the step response sequences studied, transient mode is only activated for a few seconds in the beginning of the step response. Therefore the deviation in EGR rate will not be significant for the overall results. In transient test cycles such as the ETC or WHTC, transient mode is more frequently activated and the problem with poor agreement between reference and actual EGR rate will be more pronounced.
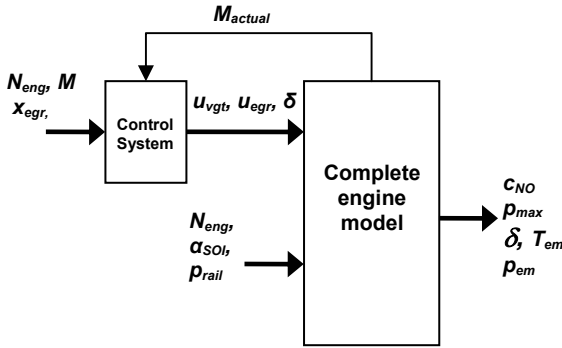
**Figure 2.9 Complete engine model with simplified control system.**

### 2.3.2 Static Engine Model

In some cases, such as the MPC application discussed in Chapter 6, the computational performance of the complete engine model is inadequate. In order to study the effects of varying EGR rate and injection timing, a set of 4D-look up tables are created:

$$\delta = \delta\left(N_{eng}, M, \alpha_{SOI}, x_{egr}\right) \tag{2.56}$$

$$y_{NO} = y_{NO}\left(N_{eng}, M, \alpha_{SOI}, x_{egr}\right) \tag{2.57}$$

$$W_{trb} = W_{trb}\left(N_{eng}, M, \alpha_{SOI}, x_{egr}\right) \tag{2.58}$$

$$T_{em} = T_{em}\left(N_{eng}, M, \alpha_{SOI}, x_{egr}\right) \tag{2.59}$$

$$p_{em} = p_{em}\left(N_{eng}, M, \alpha_{SOI}, x_{egr}\right) \tag{2.60}$$

The look up tables are based on a steady state calibration of the entire operating range of the engine. For a given injection timing, EGR rate, engine speed and torque, brake specific fuel consumption is minimized as a function of VGT actuator position and EGR valve position (using the complete model). A maximum cylinder pressure constraint is also added. Fuel rail pressure is not an optimization parameter; instead it is calculated as a linearly increasing function of EGR rate. Since no model for engine out PM emissions is included in the complete model, rail pressure is chosen to ensure low PM levels based on measurement data. The data in the look up tables is smoothed in order to avoid local minima.

A comparison between the complete and static engine models is given in Figure 2.10. In this comparison, the reference EGR rate is fed directly to the combustion model in the complete model case. Otherwise, a large difference between the model outputs will relate to the deviance between reference and actual EGR rate as discussed in Section 2.3.1. Note that the simplified control system is still used to obtain inputs to the gas exchange model; this will have a slight impact on other quantities such as exhaust mass flow and inlet manifold pressure. Only the EGR rate calculation in the gas exchange model is bypassed. Two outputs from the SCR model (presented in Chapter 4) are also given, $NO_x$ and $NH_3$ fraction after the catalyst. In general some transient deviation can be seen in the exhaust mass flow as a result of neglecting the gas exchange dynamics in the static model. More consistent errors are apparent at a few instances (~1300 s and ~1700 s) as a result of an insufficiently dense discretization of the look up tables. The shift of the $NH_3$ peak is related to a slightly higher exhaust temperature with the static model. The overall agreement between the two models is acceptable however, making the static model suitable in applications where the complete model is too computationally heavy. Another option would be to use a simplified method analogously to Schär et al. [18] where the transient $NO_x$ emissions are described as a first order system with steady state values given by a look up table. The general use of look up tables in transient operation, "quasi stationary models", is discussed in more detail in paper I.
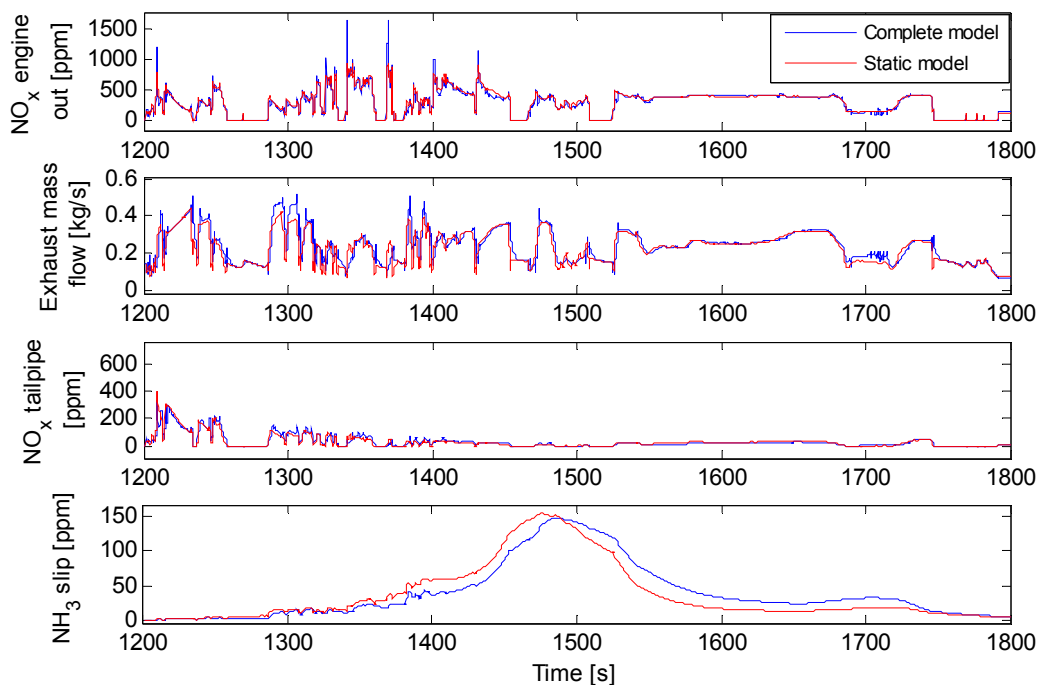


**Figure 2.10 Comparison complete vs. static engine model, sequence of the WHTC.**

# 3 Exhaust System Model

The exhaust gas expansion will continue from the exhaust manifold over the turbine to almost ambient pressure in the exhaust system. The temperature after the engine is given by:

$$T_{exh} = T_{em} \cdot \left( \frac{p_{amb}}{p_{em}} \right)^{\frac{\gamma_{atrb} - 1}{\gamma_{atrb}}}$$

(3.1)

Note that this temperature is not identical to the post turbine temperature used in the gas exchange model, Equation (2.52). The polytropic exponent in Equation (3.1) is tuned to make the pre catalyst temperature, Equation (3.6), a good fit to measurements. The exhaust temperature will be further reduced and low pass filtered prior to reaching the silencer/catalyst. This is related to heat transfer to and from the exhaust system. A dynamic mean value exhaust system model is presented by Eriksson [19]. This model is used in the engine model in a simplified form; heat conduction between engine and exhaust system and radiative heat transfer is neglected. The exhaust system energy balance is given by:

$$\frac{dT_w}{dt} m_{exh.sys} c_{p,exh.sys} = A_{exh.sys} \left( h_{gi} \left( T_{exh} - T_w \right) - h_{cve} \left( T_w - T_{amb} \right) \right)$$

(3.2)

where $m_{exh.sys}$, $c_{p,exh.sys}$, $A_{exh.sys}$ are the mass, specific heat and inner/outer surface area (assumed equal) of the exhaust system. $T_w$ is the exhaust system wall temperature. The external convection heat transfer coefficient, $h_{cve}$ is assumed to be constant. The generalized internal heat transfer coefficient is given by [19]:

$$h_{gi} = \frac{1 - e^{-\frac{h_{cvi} A_{exh.sys}}{W_{trb} c_{p,exh}}}}{\frac{h_{cvi} A_{exh.sys}}{W_{trb} c_{p,exh}}} h_{cvi}$$

(3.3)

The internal convective heat transfer coefficient is highly flow dependent, and is estimated using the Nusselt number:

$$h_{cvi} = \frac{Nu \lambda_{exh}}{d_{exh.sys}}$$

(3.4)

where the Nusselt number is estimated using the following relation [19]:

$$Nu = 0.48 Re^{0.5}$$

(3.5)

The pre-silencer/catalyst temperature is given by:

$$T_{precat} = T_w + \left( T_{exh} - T_w \right) e^{\frac{h_{cvi} A_{exh.sys}}{W_{trb} c_{p,exh}}}$$

(3.6)

# 4 SCR Catalyst Model

In this chapter, a model of a vanadia based SCR catalyst of typical heavy truck dimensions is presented. The studied catalyst has a homogenous structure, i.e. the active material is distributed throughout the entire catalyst wall. First, a brief literature survey is given.

## 4.1 Literature Survey

Tronconi et al. [20] discuss the use of lumped parameter (one dimensional) models of monolithic SCR catalysts. The local Sherwood number is estimated using the analogy with the Graetz-Nusselt heat transfer problem with constant wall temperature. This approach neglects the influence of kinetics on mass transfer coefficients. It is shown however that using first order as well as Eley-Rideal kinetics, the agreement with a more comprehensive two dimensional model and measurement data is good. Steady state operation only is considered. This type of lumped parameter approach is the basis for most work in SCR catalyst modelling.

One of the first attempts to model a vanadia based SCR catalyst for diesel applications in transient operation is described by Andersson et al. [21]. The mechanism described is the reaction between adsorbed $NH_3$ and gas phase NO, i.e. Eley-Rideal kinetics. The reaction mechanism involves the DeNOx reaction, adsorption/desorption of $NH_3$ and $NH_3$ oxidation. The film model is used to model the mass transfer between the gas bulk and catalyst surface while diffusion resistance in the washcoat is neglected. The activation energy for $NH_3$ desorption is modelled using a modified Temkin-type coverage dependency. The catalyst is discretized in the axial direction to simplify the solution. Reasonable agreement is shown with measurements.

The model is further developed by Andersson [22]. SCR catalysts of the coated and incorporated (homogenous) type are compared. In particular for the latter type it is identified that internal mass transport (diffusion resistance in the catalyst wall) can not be neglected.

A similar model is presented by Chatterjee et al. [23]. Practically the same reaction mechanism is used, although inhibition of $NH_3$ on the DeNOx reaction is considered using Langmuir-Hinshelwood kinetics. The inhibition is demonstrated using microreactor experiments, although the relevance to real world operation can be questioned considering the low $H_2O$ fraction used. Also, the inhibition effect will be amplified in the experiment due to the high inlet $NH_3$ fraction (almost three times larger than the possible NO conversion); therefore the surface coverage will be unrealistically high. In accordance with Andersson [22], the authors stress the importance of modelling intraporous mass transport limitations.

More recently, Nova et al. [24] studied the mechanism of the $NO_2$ augmented "Fast SCR" reaction. Using microreactor experiments, a reaction mechanism is identified which involves $HNO_3$ and $NH_4NO_3$ intermediates. The work is extended by Chatterjee et al. [25] where the model in [23] is improved with the new reactions. Model states for six gaseous species ($NH_3$, NO, $NO_2$, $N_2$, $N_2O$ and $HNO_3$) and two adsorbed species ($NH_3$, $NH_4NO_3$) are included.

## 4.2  Model Structure

The catalyst is modelled as a series of continuously stirred tank reactors. The walls are discretized into a number of layers to describe the mass transport through the walls, as illustrated in Figure 4.1. The model uses two wall layers and six segments (tanks) in the axial direction. One temperature state in each tank and one ammonia coverage in each wall layer results in a total of 18 states. This is a less dense discretization than traditionally used, for example, Westerberg et al. use 10 tanks in the axial direction [26], Andersson et al. [21] use 33 tanks. Devarakonda et al. [27] conclude that no more than 15 tanks are necessary in the higher order model presented. In the other end of the spectrum, the more control oriented model presented by Schär et al. [18] use 2 tanks and the reduced order model of Devarakonda et al. [27] use a single tank. Such sparse discretizations do sacrifice good agreement with measurements however. The choice of six tanks is a good compromise between accuracy and computational efficiency. The importance of including mass transfer in the catalyst wall is discussed in Section 4.1; no less than two wall layers can thus be used. A comparison between two and three wall layers is presented in paper III.
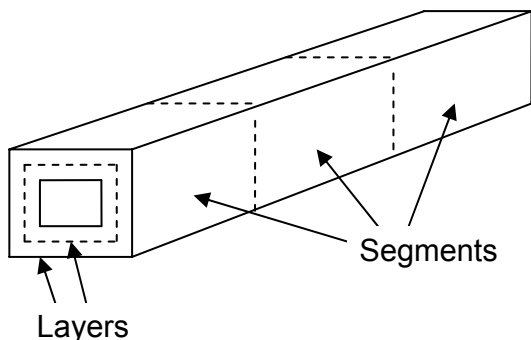


**Figure 4.1  Illustration of the catalyst discretization principle.**

Axial diffusion and radial temperature gradients are both neglected. Uniform radial flow and concentration distribution over the catalyst cross section is assumed; therefore it is sufficient to model one channel only. When discussing uniformity, three different effects can be separated:

1. Reduction agent distribution
2. Flow distribution
3. Temperature distribution

The reduction agent distribution is the most important; catalyst channels with too much reduction agent will result in $NH_3$ slip and the channels with too little will have insufficient $NO_x$ reduction. Non uniform distribution of the reduction agent is not possible to compensate for by over dosing $NH_3$. The flow distribution will not be of great significance, channels with flow velocity below average will achieve $NO_x$ reduction which is higher than average and lower reduction is achieved where the flow is higher. The average will not quite sum up, but is usually close unless the uniformity is poor. Non uniformity in the temperature distribution will, analogously with the flow distribution, approximately even out. Recent SCR applications, aiming for Euro V or Euro VI emissions, are designed with uniformity issues in mind in order to achieve the performance required.

## 4.3 Reactions

The reaction mechanism consists of five reactions:

$$CO(NH_2)_2 + H_2O \rightarrow 2NH_3 + CO_2 \tag{4.1}$$

$$S + NH_3 \rightarrow S - NH_3 \tag{4.2}$$

$$S - NH_3 \rightarrow S + NH_3 \tag{4.3}$$

$$2S - NH_3 + 2NO + \frac{1}{2}O_2 \rightarrow 2S + 2N_2 + 3H_2O \tag{4.4}$$

$$2S - NH_3 + \frac{5}{2}O_2 \rightarrow 2S + 2H_2O + 2NO \tag{4.5}$$
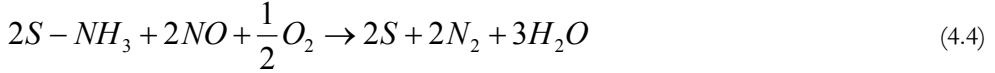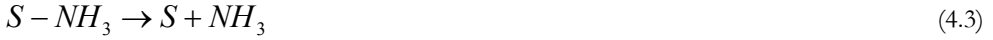
$S$ denotes an active site on the catalyst surface. Reaction 1, Equation (4.1), describes the decomposition of urea to ammonia. This is a simplification; the actual decomposition consists of two reactions. First the urea is decomposed in gas phase to equimolar amounts of ammonia and isocyanic acid (thermolysis). Then the isocyanic acid is hydrolyzed to ammonia on the catalyst surface. This step is generally considered to be fast compared to the thermolysis; therefore it is a reasonable assumption to treat the isocyanic acid as ammonia. The adsorption/desorption (accumulation) of ammonia is given by reactions 2 and 3 (Equations (4.2) and (4.3)). Traditionally, the activation energy for desorption of ammonia is considered to be reduced with increasing coverage. Different methods have been used to model this dependency, for example Temkin-type (linear decrease) or Freundlich-type (exponential decrease) [28]. Another approach is to use two different types of sites with different activation energies. In the kinetic model given here however where computational performance is highly prioritized, only one site type is used with constant activation energies. The desired reaction, NO reduction on the active sites is described by reaction 4, Equation (4.4). Finally, at higher temperatures, unwanted ammonia oxidation also occurs on the sites, reaction 5, Equation (4.5). The corresponding reaction rates are given by:

$$r_1 = k_1 c_{Urea} \tag{4.6}$$

$$r_2 = k_2 c_{NH_3} \left(1 - \theta_{NH_3}\right) \tag{4.7}$$

$$r_3 = k_3 \theta_{NH_3} \tag{4.8}$$

$$r_4 = k_4 c_{NO} \theta_{NH_3} \tag{4.9}$$

$$r_5 = k_5 \theta_{NH_3} \tag{4.10}$$

The rate coefficients $k_j$ are calculated using an Arrhenius type expression:

$$k_j = k_{0,j} e^{-\frac{E_{A,j}}{RT_S}} \tag{4.11}$$

where $j$ is reaction number, $k_{0,j}$ is the preexponential factor, $E_{A,j}$ is the activation energy, $R$ is the molar gas constant and $T_S$ is the surface temperature.

## 4.4 Mass and Heat Balances

The axial flow and the radial diffusion are both modelled using static balance equations for the gas phase and time dependent balances for the solid catalyst.
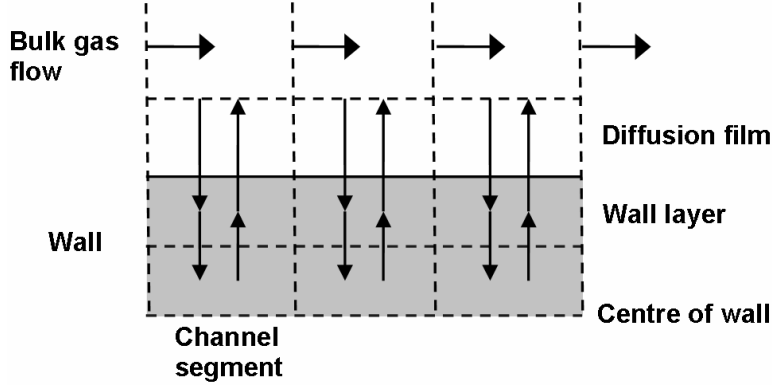


**Figure 4.2 Illustration of mass transport in the catalyst channel.**

The gas phase mass transport is illustrated in Figure 4.2 and is given mathematically by the following relations:

$$F_{tot}(y_{i,k-1} - y_{i,k}) - \Gamma_{i,k,0}(c_{i,k,0} - c_{i,k,1}) = 0 \tag{4.12}$$

$$\Gamma_{i,k,n-1}(c_{i,k,n-1} - c_{i,k,n}) - \Gamma_{i,k,n}(c_{i,k,n} - c_{i,k,n+1}) + \sum_j \nu_{i,j} r_{j,k,n} w_{k,n} = 0 \quad for \quad n \geq 1 \tag{4.13}$$

where $F_{tot}$ is the total molar flow $c_{i,k,n}$ is the concentration of component $i$ in channel segment $k$ and wall layer $n$ (where $n=0$ indicates gas bulk and $n>0$ indicates wall) and $w_{k,n}$ is the mass of catalyst material in channel segment $k$ and wall layer $n$. The mass transfer coefficients $\Gamma_{i,k,n}$ are given by:

$$\Gamma_{i,k,0} = \frac{A_k}{\dfrac{1}{k_{c,i,k}} + \dfrac{0.5\Delta x_1}{D_{eff,i,k}}} \tag{4.14}$$

$$\Gamma_{i,k,n} = \frac{D_{eff,i,k} A_k}{0.5\Delta x_n + 0.5\Delta x_{n+1}} \quad for \quad n = 1 \quad \dots \quad N-1 \tag{4.15}$$

$$\Gamma_{i,k,N} = 0 \tag{4.16}$$

where $A_k$ is the mass and heat transfer area in channel segment $k$. For simplicity reasons, $A_k$ is assumed to be constant for all wall layers.

The parameter $D_{eff,i,k}$ is the effective pore diffusion coefficient of specie $i$ in channel segment $k$, $k_{c,i,k}$ is the film transfer coefficient of component $i$ in channel segment $k$ and $\Delta x_n$ is the thickness of wall layer $n$. The gas energy balance is given by:

$$F_{tot} c_{p,g} (T_{g,k-1} - T_{g,k}) - h_k A_k (T_{g,k} - T_{s,k}) = 0 \qquad (4.17)$$

where $c_{p,g}$ is the specific heat capacity for the gas, $h_k$ is the heat transfer coefficient in channel segment $k$, $T_{g,k}$ and $T_{s,k}$ are the temperatures in channel segment $k$ in the gas bulk and of the catalyst respectively. The solid energy balance is given by:

$$m_{s,k} c_{p,s} \frac{dT_{s,k}}{dt} = h_k A_k (T_{g,k} - T_{s,k}) - A_s (q_{k+1} - q_k) + \sum_n \sum_j r_{j,k,n} w_{k,n} (-\Delta H_j)$$

$$(4.18)$$

where $m_{s,k}$ is the total mass of solid material in channel segment $k$, $c_{p,s}$ is the heat capacity of the solid material, $A_s$ is the cross sectional area of the catalyst wall, $w_{k,n}$ is the mass of active catalyst material in channel segment $k$ and wall layer $n$ and $-\Delta H_j$ is the heat of reaction $j$. The solid heat flux is calculated as:

$$q_k = -2\lambda_s \frac{T_{s,k} - T_{s,k-1}}{\Delta z_k + \Delta z_{k-1}} \quad for \quad k = 2 \ldots K-1, K \qquad (4.19)$$

$$q_k = 0 \quad for \quad k = 1, K+1 \qquad (4.20)$$

where $\lambda_s$ is the heat conductivity for the solid material, $\Delta z_k$ is the length of channel segment $k$ and $K$ is the total number of channel segments. The mass and heat transfer is described with the film model and the mass and heat transfer coefficients are given by:

$$k_{c,i,k} = \frac{Sh D_{i,k}}{d} \qquad (4.21)$$

$$h_k = \frac{Nu \lambda_{exh}}{d} \qquad (4.22)$$

where $D_{i,k}$ is the diffusion coefficient for component $i$ in channel segment $k$, $\lambda_{g,k}$ is the gas heat conductivity in channel segment $k$ and $d$ is the channel width. The Sherwood number, $Sh$, is calculated using the Graetz-Nusselt analogy [20]:

$$Sh = Sh_\infty + 6.874 \cdot (1000 \cdot z^*) \cdot e^{-57.2 z^*} \qquad (4.23)$$

where $z^*$ is the dimensionless axial distance given by:

$$z^* = \frac{z \cdot D_{i,k}}{u_{channel} \cdot d^2} \qquad (4.24)$$

In Equation (4.24), the axial distance $z$ is normalized using the diffusion coefficient $D_{i,k}$, the exhaust gas velocity $u_{channel}$ and the channel width $d$. The Nusselt number, $Nu$, is calculated analogously.

The surface mass balance for segment $k$ and layer $n$ is given by:

$$\frac{d\theta_{NH_3,k,n}}{dt} = \frac{1}{N_c}\left(r_{2,k,n}(t) - r_{3,k,n}(t) - 2r_{4,k,n}(t) - 2r_{5,k,n}(t)\right) \tag{4.25}$$

The differential equation is usually solved using the Euler method. This requires short time step lengths, less than 50 ms in order to retain stability at higher temperatures. High order solvers do allow longer step lengths, but the overall computational performance is not significantly improved.

### 4.4.1    Implicit ODE Solver

Using implicit methods, more accurate steps are obtained which allows for longer time step lengths. The implicit calculations applied in the SCR model use the second layer concentrations and surface temperatures from the previous time step. Combining the updated first layer coverage according to:

$$\theta_{NH_3,k,1}(t + \Delta t) = \theta_{NH_3,k,1}(t) + \Delta t \frac{d\theta_{NH_3,k,1}}{dt} \tag{4.26}$$

with Equations (4.12)-(4.13) and (4.25), the result is a third degree polynomial:

$$\beta_1\left(\frac{d\theta_{NH_3,k,1}}{dt}\right)^3 + \beta_2\left(\frac{d\theta_{NH_3,k,1}}{dt}\right)^2 + \beta_3\left(\frac{d\theta_{NH_3,k,1}}{dt}\right) + \beta_4 = 0 \tag{4.27}$$

where

$$\beta_m = \beta_m\left(\Delta t, \theta_{NH_3,k,1}(t), c_{i,k-1,0}(t + \Delta t), c_{i,k-1,2}(t), F(t + \Delta t), T_S(t)\right) \tag{4.28}$$

The cubic equation is easily solved analytically using Cardanos method. Choosing which root to use is simple; only one is physically possible.

### 4.4.2    First Order Simplification

Another method to improve high temperature stability is to simplify the system to a first order system approaching a steady state solution $\theta_{ss}$ in each time step [29]. The coverage is given by:

$$\frac{d\theta_{NH_3,k,1}}{dt} = \frac{\theta_{NH_3,ss,k,1} - \theta_{NH_3,k,1}}{\tau} \tag{4.29}$$

where $\theta_{NH3,ss,k,1}$ is the steady state solution corresponding to the current inputs and $\tau$ is a characteristic time constant.

The steady state solution can be estimated by solving a simplified version of the gas phase mass balances, Equations (4.12)-(4.13). The method presented in paper III, only works accurately at high temperatures (>700K) due to the assumption of severe mass transport limitations. This is not a problem in the first order simplification. The MPC controller presented in paper V/Section 6.4.1 solves an optimization problem to set the end of simulation $NH_3$ coverage constraint, Equation (6.13). This requires a new simplified solution which works accurately at all temperatures. The new method, first described in paper V, uses an internal effectiveness factor to simplify the calculations. A similar approach is used in an oxidation catalyst model by Chatterjee et al. [30]. In a SCR catalyst model however, the $NH_3$ adsorption/desorption makes the internal effectiveness factor useable for modelling purposes in steady state only. The internal effectiveness factor is defined as the ratio of actual molar flow at the surface and the molar flow in the absence of diffusion resistance [31,32], i.e. controlled by reaction kinetics only.

The internal effectiveness factor is given by:

$$\eta_{i,k} = \frac{\sum_{n=1}^{N} r_{i,k,n} w_{k,n}}{r_{i,k,1} \sum_{n=1}^{N} w_{k,n}} \tag{4.30}$$

where $w_{k,n}$ is the mass of catalyst material in channel segment $k$ and wall layer $n$.

The internal effectiveness factor is dependent on the relation between the diffusion rate and the reaction rate. At high temperatures, the reaction rate is high compared to the diffusion rate resulting in a low effectiveness factor and at low temperatures the opposite case results in a high internal effectiveness factor. The absolute values of the molar fractions/concentrations of the different species can approximately be considered to cancel out in Equation (4.30). The internal effectiveness factor is therefore primarily related to temperature; both the diffusion coefficients and the rate coefficients are temperature dependent only. Figure 4.3 shows simulated internal effectiveness factors from the entire operating range of the steady state calibration of the engine (described in Chapter 6.1). As expected, a good correlation is observed between the internal effectiveness factor and catalyst temperature. Above ~500 K, the internal effectiveness factor approaches the asymptotic value; the mass fraction of the first wall layer. Note that these observations are not generally applicable. First, the results are only valid for the (sparse) discretization used. Secondly, even though the data which Figure 4.3 is based on has a limited range of inlet concentrations, some variations can still be seen. If a wider range of operating conditions are to be considered, the correlation to temperature only would be less accurate.

**Figure 4.3 Internal effectiveness factor, reaction 4.**

Internal effectiveness factor look up tables for all reactions are created by interpolating the data in Figure 4.3:

$$\eta_i = \eta_i(T_S) \tag{4.31}$$

Using the internal effectiveness factor tables, the gas phase mass balances combined with equilibrium in the surface mass balance (neglecting reaction 5) results in a second order equation for equilibrium $NH_3$ coverage:

$$g_{\theta_{ss},1}\theta_{NH_3,ss,k,1}^{\;2} + g_{\theta_{ss},2}\theta_{NH_3,ss,k,1} + g_{\theta_{ss},2} = 0 \tag{4.32}$$

where

$$g_{\theta_{ss},m} = g_{\theta_{ss},m}\left(c_{NO,k-1,0}, c_{NH_3,k-1,0}, c_{Urea,k-1,0}, F_{tot}, T_S\right) \tag{4.33}$$

The result is an analytical steady state solution of the SCR catalyst model valid at all temperatures. Only one solution to Equation (4.32) is physically possible. The time constant is estimated using a black box model:

$$\tau_{k,1} = \tau_{k,1}\left(T_{s,k}, \theta_{NH_3,ss,k,1}, c_{NO,k,1}, c_{NH_3,k,1}, c_{urea,k,1}\right) \tag{4.34}$$

The implicit method is combined with the first order simplification in the model with a switching point of 720K (Figure 4.4)

$$\frac{d\theta_{NH_3,k,1}}{dt} = \frac{\theta_{ss,k,1} - \theta_{NH_3,k,1}}{\tau}$$

$$\theta_{NH_3,k,2} = 0$$

$$\frac{d\theta_{NH_3,k,1}}{dt} = f(\beta_1, \beta_2, \beta_3, \beta_4)$$

$$\frac{d\theta_{NH_3,k,2}}{dt} = \frac{1}{N_c}\sum_j \nu_{NH_3,j} r_{j,k,2}$$
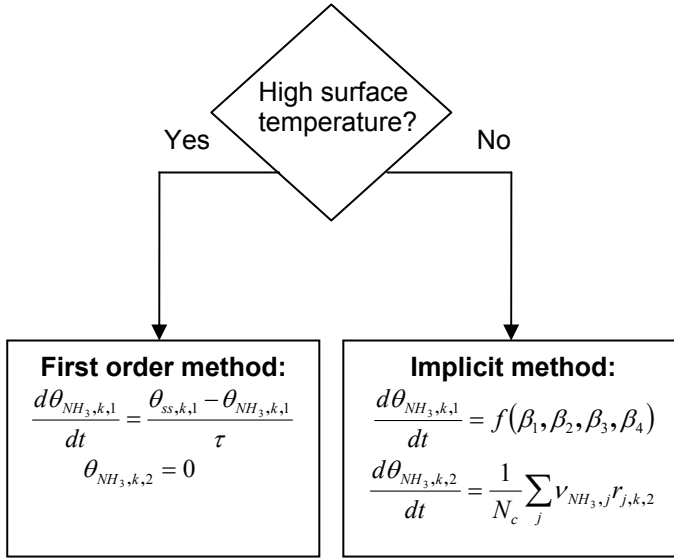
**Figure 4.4 Illustration of the two different ODE solvers.**

### 4.4.3   Diffusivity

The gas diffusivity for each component $i$ is calculated using a simplified form of the Fuller-Schettlet-Giddins equation [29]:

$$D_i = D_{ref,i}\left[\frac{T_s}{T_{ref}}\right]^{1.75} \tag{4.35}$$

where $T_{ref}$ is a reference temperature.

The effective diffusivity for pore diffusion is given as:

$$D_{eff,i} = \frac{f_D}{\dfrac{1}{D_i} + \dfrac{1}{D_{K,i}}} \tag{4.36}$$

$f_D$ is a factor that takes into consideration the porosity and the tortuosity of the porous material. $D_{K,i}$ is the Knudsen diffusivity which is calculated as [29]:

$$D_{K,i} = \frac{d_p}{3}\sqrt{\frac{8RT_s}{\pi M_i}} \tag{4.37}$$

where $d_p$ is the mean pore diameter.

## 4.5  Urea Decomposition Before the Catalyst

Heating the urea to exhaust temperature and vaporizing it will result in a temperature drop according to:

$$T_{cat,in} = T_{precat} - \frac{y_{urea}}{c_{p,exh}} \left( H_{v,urea} + x_{H_2O} H_{v,H_2O} + \left( c_{p,urea} + x_{H_2O} c_{p,H_2O} \right) \left( T_{precat} - T_{amb} \right) \right)$$

(4.38)

$x_{H_2O}$ is the molar ratio of water to urea and $H_{v,urea} / H_{v,H_2O}$ is the heat of vaporization of urea/water. Thermolysis will also occur in the gas phase after the urea injection and before the catalyst. A first order reaction mechanism is applied:

$$r_{precat} = k_{precat} c_{urea}$$

(4.39)

The rate coefficient is given by:

$$k_{precat} = k_{0,precat} e^{-\frac{E_{A,precat}}{R T_{cat,in}}}$$

(4.40)

The conversion is calculated using a tubular reactor model for the empty section of the exhaust system:

$$x_{urea} = 1 - e^{\frac{k_{precat} V_{precat}}{W_{trb}}}$$

(4.41)

where $V_{precat}$ is the exhaust system volume between the injector and the catalyst inlet and $W_{exh}$ is the total exhaust gas mass flow.

# 5 Complete Model

The previously described engine, exhaust system and SCR catalyst models are combined to form a complete model of the system.
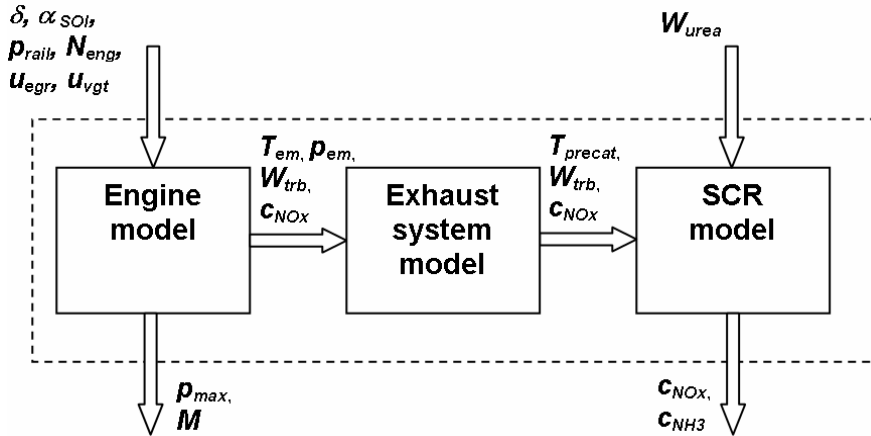
## 5.1 Model Structure



**Figure 5.1 Model structure.**

The model structure of the complete model is given in Figure 5.1. The only inputs required are the typical engine control parameters. Torque, $NO_x$ concentration, $NH_3$ slip and peak cylinder pressure are given as outputs. The computational performance is limited by the engine model, i.e. ~10 X real time.

## 5.2 Validation

The complete model is validated using measurements from the engine test bed on a European Transient Test Cycle (ETC). Injected fuel amount, injection timing, rail pressure and EGR/VGT actuator signals are given in the measurements, i.e. the simplified control system (Section 2.3.1) is not used. A comparison of measured and simulated values is given in Figure 5.2. The emissions measurement technique results in low pass filtering of the signals. In order to get a good comparison with measurements, the simulated data ($NO_x$ and $NH_3$) is low pass filtered to emulate the dynamics of the measurement system. The agreement is quite good, specific $NO_x$ engine out for the test cycle is predicted with a -8.5 % relative error. As discussed by Ericson [17], the relative error in $NO_x$ and $NH_3$ after the catalyst is not a relevant measure on the performance of the SCR catalyst model due to the low absolute values. The error sources in the experiment will have a greater influence than the model errors. For example, the tolerance of the urea injection system is far greater than the absolute deviation between measurements and model outputs post catalyst. Specific $NO_x$ after the catalyst shows a relative error of +10 % and mean $NH_3$ slip is predicted with a +13 % relative error. More relevant measures are $NO_x$ conversion over the SCR catalyst, which is underpredicted with only 4.0 %, and mean $NH_3$ slip relative to injected $NH_3$ which is overpredicted with 1.0 %.
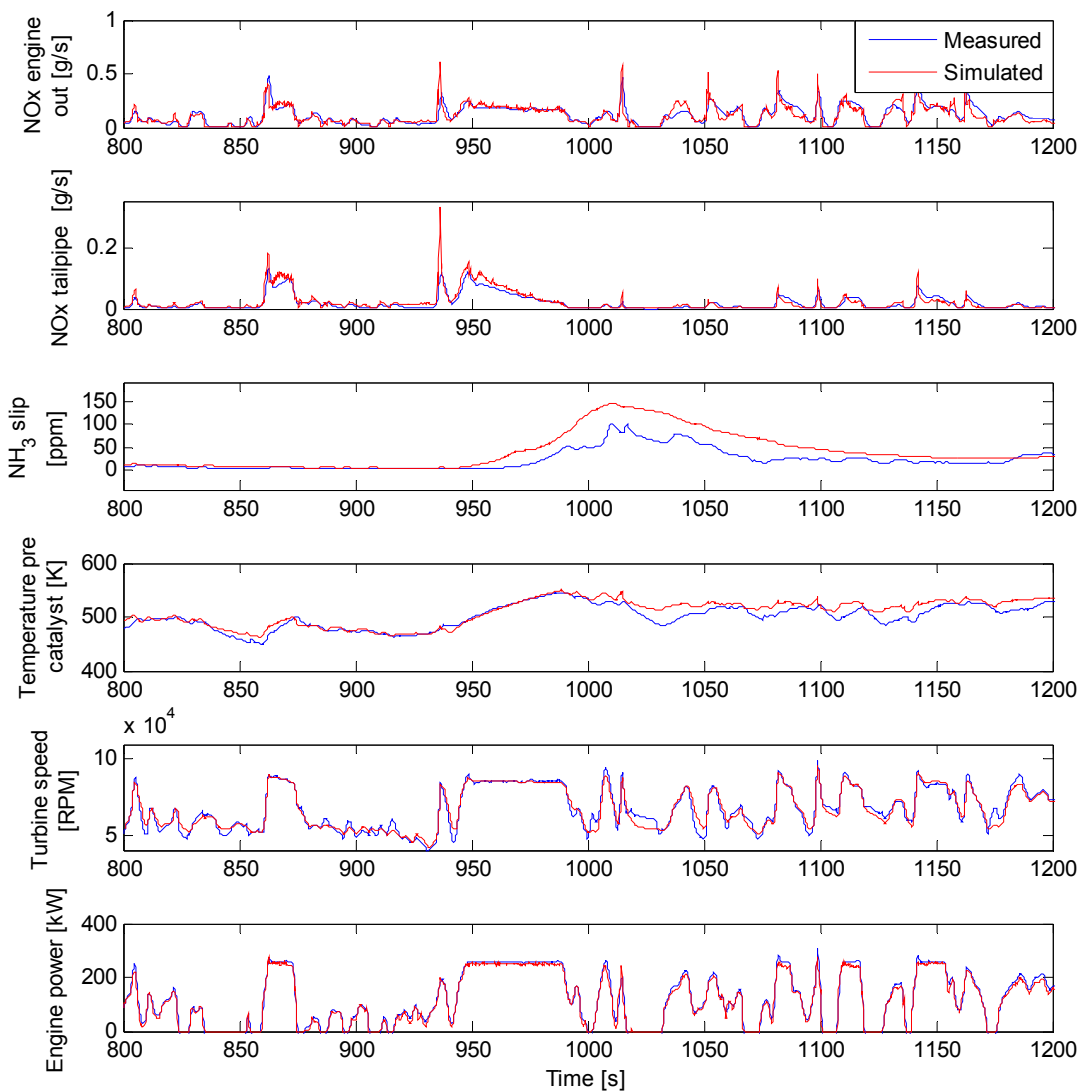
**Figure 5.2 Validation complete model, sequence of the ETC.**

# 6 Model Based Optimization

The model based optimization work is presented in this chapter. First, a literature survey on previous work in the area is given.

## 6.1 Literature Survey

In recent years, a number of papers have been published on the topic model based control/optimization of the SCR system. A selection of this work is presented here.

Upadhyay et al. [33] presents a model based controller using optimal control theory. An observerer is designed using measured $NO_x$ after the SCR catalyst for estimation. In order to make use of the observer, the model is very simple; the whole catalyst is modelled as a single continuously stirred tank and mass transfer is neglected.

Devarakonda et al. [34] presents an extension of the work in [33]. The updated model involves both the "fast SCR" reaction involving $NO_2$ and the "standard SCR" reaction. A control strategy which explores the $NO_2$ reaction is presented which offers improved performance over previous control strategies. The simple model shows reasonable agreement with measurements during stationary conditions but during rapid transients the agreement is poor. This is expected because no discretization in the axial direction is used in the catalyst model. The performance of the controller is somewhat questionable, showing unacceptably high levels of $NH_3$ slip in the FTP cycle.

Schär et al. [18] describes a controller based on a simplified model using feedforward and feedback control using a $NO_x$ sensor. The model used is similar to reference [33] except for a catalyst discretization with two segments in the axial direction. Different feedforward controllers designed to limit transient $NH_3$ slip are presented and a feedback controller is added to handle disturbances. The overall results are quite good with $NH_3$ slip below 10 ppm and a $NO_x$ reduction of 87% in the ETC.

Chi et al. [35] presents a more advanced SCR catalyst model than the previous two references. The catalyst channel is discretized axially and radially in a similar manner as the model presented in this thesis in Chapter 4. The model based controller presented, uses a simple first order simplification of the system however. The parameters in the first order model are estimated online using a model-reference adaptive controller. The results are good, 84% $NO_x$ reduction with a mean $NH_3$ slip of 7 ppm is achieved in the FTP test cycle.

No work using a complete system approach has been found however, i.e. controlling engine out $NO_x$ and $NO_x$ reduction over the SCR catalyst simultaneously.

## 6.2  Steady State Optimization

The steady state optimization problem is given by:

$$\min \ f_{BSFC}\left(\alpha_{SOI}, x_{egr}, W_{urea}\right) \tag{6.1}$$

$$\alpha_{SOI} \in \Omega_{\alpha_{SOI}}, x_{egr} \in \Omega_{egr}, W_{urea} \in \Omega_{urea}$$

$s.t.$

$$C_{NO_x}\left(\alpha_{SOI}, x_{egr}, W_{Urea}\right) \leq LD_{NO_x} \tag{6.2}$$

$$C_{NH_3}\left(\alpha_{SOI}, x_{egr}, W_{Urea}\right) \leq LD_{NH_3} \tag{6.3}$$

$$C_{\theta_{NH_3,avg}}\left(\alpha_{SOI}, x_{egr}, W_{Urea}\right) \leq \theta_{NH_3,max} \tag{6.4}$$

where Equation (6.2) is the specific $NO_x$ constraint and Equation (6.3) is the $NH_3$ slip constraint. The addition of an average $NH_3$ coverage constraint, Equation (6.4), is used as a precaution to avoid excessive $NH_3$ slip in transient operation. The target function, Equation (6.1), brake specific fuel consumption including equivalent urea cost, is given by:

$$f_{BSFC}\left(\alpha_{SOI}, x_{egr}, W_{Urea}\right) = \frac{W_{fuel}\left(\alpha_{SOI}, x_{egr}\right) + EQ_{Urea}W_{urea}}{P} \tag{6.5}$$

Using the static engine model, the fuel flow is calculated directly from Equation (2.56). Note that multiple injections are not considered in any of the optimization work presented in the thesis. Also, since no model for engine out PM emissions is included in the complete model, rail pressure is chosen to ensure low PM levels based on measurement data. The upper bounds in the constraints are set to:

$$LD_{NO_x} = 0.5 \ g/kWh$$

$$LD_{NH_3} = 10 \ ppm$$

$$\theta_{NH_3,max} = 0.75$$

Additionally, upper and lower bounds are added to the optimization variables:

$$\alpha_{SOI} \in \Omega_{\alpha_{SOI}} \tag{6.6}$$

$$x_{egr} \in \Omega_{egr} \tag{6.7}$$

$$W_{urea} \in \Omega_{urea} \tag{6.8}$$

The simplified steady state SCR catalyst model, described in Section 4.4.2, is used in the constraints function. This will save substantial optimization time compared to running the complete model.

Initial values for the optimization are given by locating the minimum BSFC plus the corresponding cost of urea to reduce $NO_x$ emissions to 0.5 g/kWh. Assuming that the SCR catalyst gives 100% conversion at all conditions, the optimum equals the initial values.
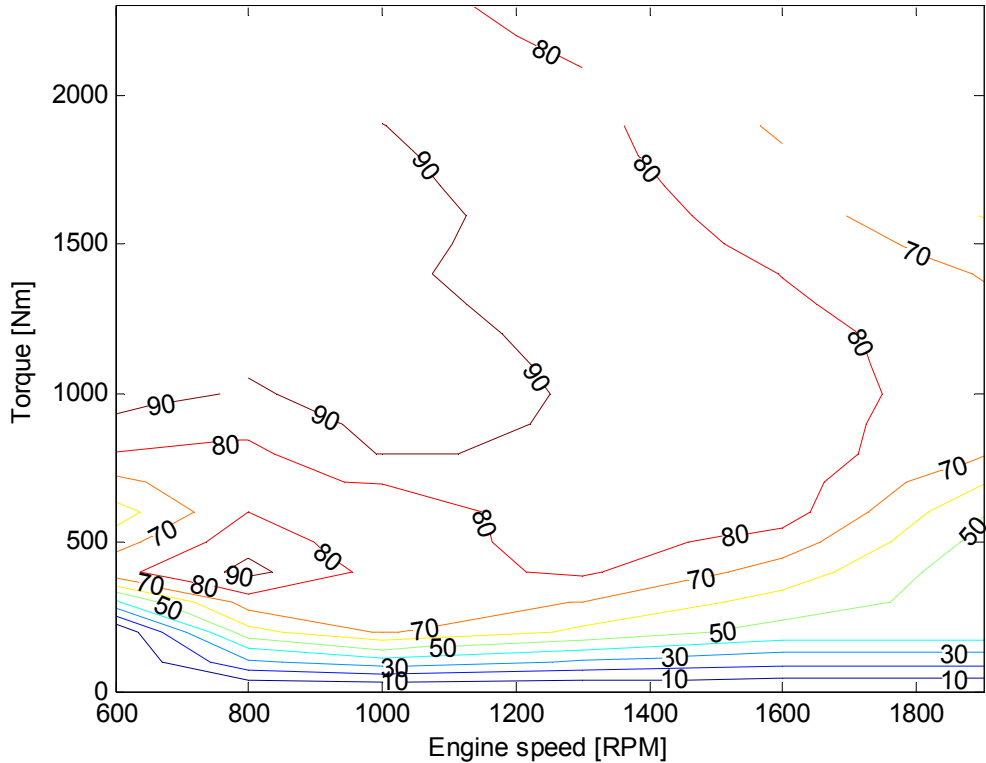


**Figure 6.1 Results of steady state optimization, $NO_x$ conversion [%].**

The results of the steady state optimization are presented in Figure 6.1. The highest $NO_x$ conversion (>90%) is achieved at low speeds and high torque, where the temperature is high. At higher speeds, the conversion is limited by excessive space velocities. At lower loads, the limiting factors are both temperature and the average $NH_3$ coverage constraint, Equation (6.4). The engine out $NO_x$ varies between 1.0 and 11.1 g/kWh depending on maximum feasible conversion and the $NO_x$/BSFC tradeoff of the operating point.

## 6.3   Characterization of Transient Operation

In paper IV, three critical operating sequences for the performance of the complete system engine plus SCR catalyst are identified:

1.   Positive load transient

2.   Negative load transient

3.   Cold start

The three cases will now be described in more detail.

### 6.3.1   Positive Load Transient

The first case is a positive load transient; as the temperature of the catalyst increases with increasing engine load, the equilibrium ammonia coverage decreases and stored ammonia will be released from the surface. An example of a load transient from 600-2300Nm at 1300 rpm is given in Figure 6.2. The steady state optimum EGR, injection timing and urea dosing values are used, i.e. no care is taken to compensate for the rising catalyst temperature, the inputs to the model are based on torque and engine speed only. The substantial $NH_3$ slip peak of almost 20 times the legislative limit must be controlled by limiting the urea dosing and possibly by increasing engine out $NO_x$. Specific $NO_x$ is lower than the steady state value of 0.5 g/kWh; this is related to the higher than equilibrium $NH_3$ coverage.
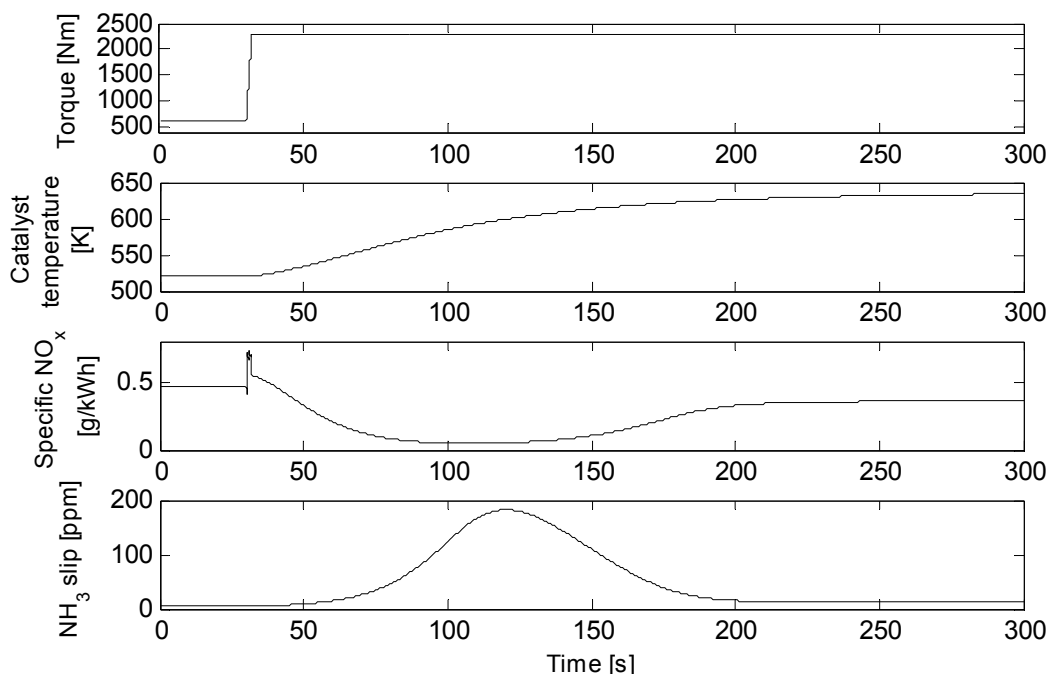


**Figure 6.2 Positive load transient, 600-2300 Nm at 1300 rpm.**

### *6.3.2   Negative Load Transient*

The second case is a negative load transient, i.e. moving from a high load to low load. The decreasing exhaust temperature (and catalyst temperature) will decrease the $NO_x$ reduction capacity of the SCR catalyst. Lower catalyst temperature also results in a higher $NH_3$ coverage equilibrium which further decreases the $NO_x$ conversion until the new equilibrium level is achieved. An example of a negative load transient is given in Figure 6.3 (the opposite of Figure 6.2). The insufficient $NO_x$ reduction can be improved by increasing the urea dosing to a higher level than the steady state optimum in order to increase the $NH_3$ coverage. Note that the urea dosing can not be overly excessive; this can result in ammonia slip. Lowering engine out $NO_x$ by increasing the EGR rate or retarding the injection timing is also useful.
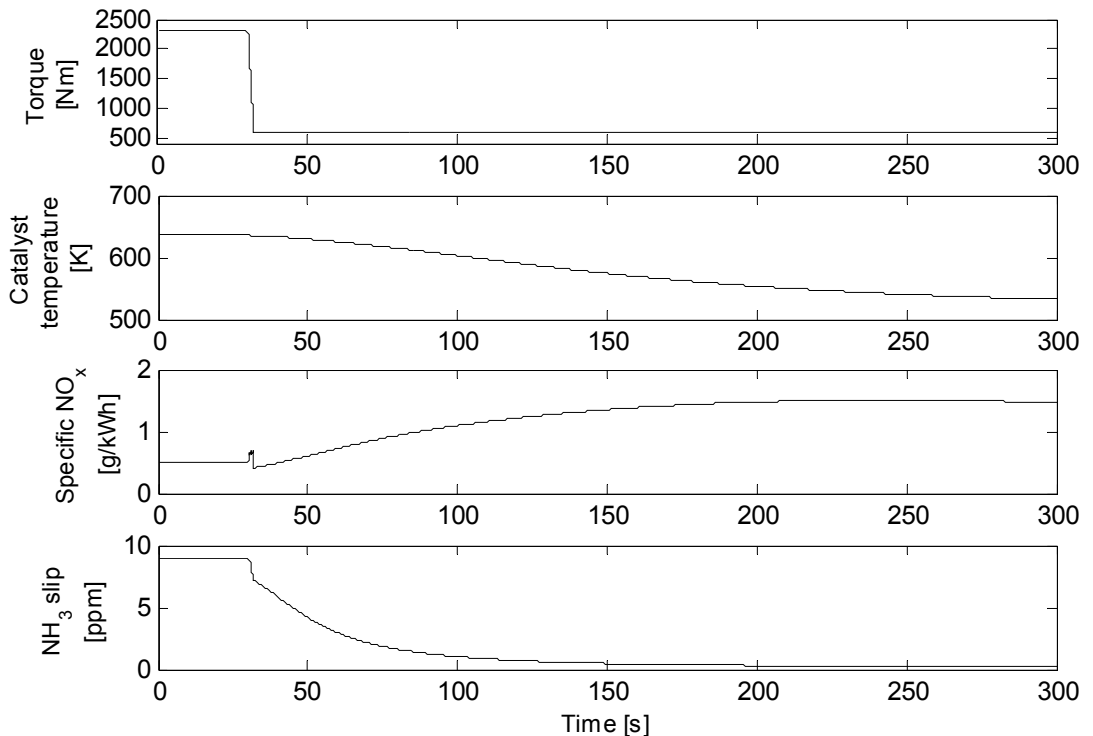


**Figure 6.3 Negative load transient, 2300-600 Nm at 1300 rpm.**

### *6.3.3   Cold Start*

The third case is a special case of case one; cold start, i.e. a positive load transient starting from ambient catalyst (and exhaust system) temperature. Apart from the lower initial temperature, the main difference between case one and three is that urea dosing will not be possible right from the start; at temperatures below 160-200 °C the urea will not be sufficiently evaporated in the exhaust stream. The approach used in this thesis is to solve the cold start problem with decreased engine out $NO_x$ and (when possible) increased urea dosing, i.e. no measures to increase exhaust temperature are explored. A more detailed discussion regarding the three critical operating sequences is given in paper IV.

## 6.4   Transient Optimization

The optimization problem formulated in paper IV is not useful for optimization of longer time sequences such as the certification test cycles (WHSC/WHTC). The problem would take excessive time to solve due to the simulation time, number of variables and number of constraints. A more suitable approach, Model Predictive Control, is described in this section. The aim of the work presented in this section is not to develop a controller based on MPC. Instead, MPC is used as a tool for optimizing transient operating conditions.

### *6.4.1   Model Predictive Control*

Model predictive control (MPC) has been used for decades in for example chemical process industries [36]. Despite the modest computational performance of the computers available, the low sampling rates in such applications made MPC viable. Normally, the models used are simple linear models combined with feedback to compensate for model errors. Recently, with rapidly increasing CPU performance available at low cost, not only is non-linear MPC (NMPC) becoming realistic, but also the higher sampling rates required in for example automotive applications. The basic working principle of a MPC controller is illustrated in Figure 6.4.
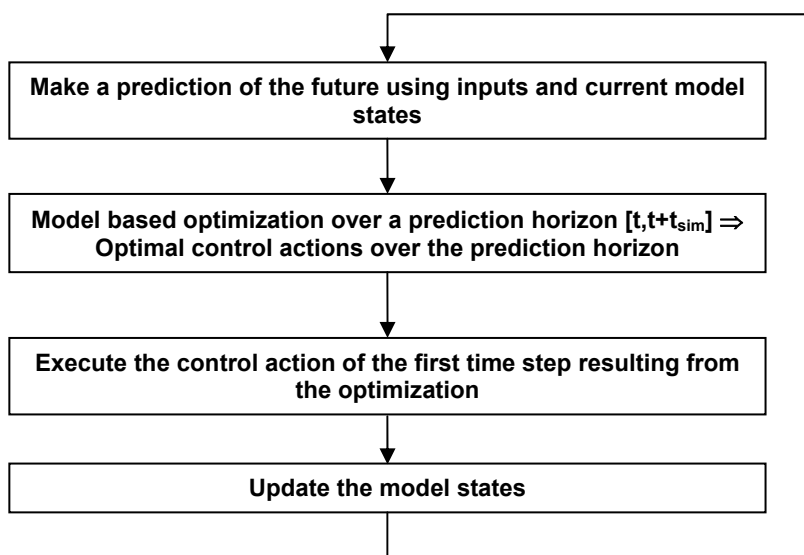


**Figure 6.4 Flowchart of the MPC principle.**

Considering the slow dynamics of the SCR catalyst, MPC is a suitable tool for control/optimization of transient sequences. The delayed response of the $NH_3$ slip and low $NO_x$ conversion observed in Figure 6.2 and Figure 6.3 can effectively be handled with constraints and a sufficiently long prediction horizon in the MPC optimization problem. Also note that the optimization problem solved in each time step of the MPC is similar to the step response optimizations performed in paper IV.

Predicting future inputs to the model (engine speed and torque) can be done in various ways. The simplest method is to assume that the current speed/torque remains constant throughout the prediction horizon. Another option is to use gradient information i.e. extrapolation using the current speed/torque gradients. Improved performance could probably be achieved by combining the MPC with look-ahead information based on map information in a similar manner as the cruise control application by Hellström et al. [37]. In this thesis however, only the first method is used, i.e. constant speed/torque during the prediction horizon.

In order to reduce optimization time, a number of simplifications have been made to the problem compared to the step response optimizations in paper IV:

- The static engine model (Section 2.3.2) is used.

- Injection timing is fixed to the steady state value, leaving only two degrees of freedom: EGR rate and urea dosing. Fuel injection pressure is a function of EGR rate according to Section 2.3.2.

- The prediction horizon is, independent of length, discretized into five time steps, resulting in a total of ten variables. In other words, the time step lengths will vary depending on the prediction horizon.

- The first two variables (EGR rate and urea dosing at time zero) will be held constant for the duration of the control step (the first time step which is executed by the MPC).

- The constraint at the end of the prediction horizon is average $NH_3$ coverage, Equation (6.13), compared to paper IV where the entire $NH_3$ coverage profile was used. Using the average value is a less strict constraint which will allow a shorter prediction horizon, therefore reducing the optimization time.

The MPC optimization problem is formulated according to:

$$\min \; f_{BSFC}\left(x_{egr}, W_{urea}\right) \tag{6.9}$$

$$x_{egr} \in \Omega_{egr}, W_{urea} \in \Omega_{urea}$$

$s.t.$

$$
\begin{aligned}
C_{NOx}\left(x_{egr}, W_{urea}\right) &\le LD_{NOx} & M &> 0 \\
C_{NOx,idle}\left(x_{egr}, W_{urea}\right) &\le LD_{NOx,idle} & M &\le 0
\end{aligned}
\tag{6.10}
$$

$$C_{NH3}\left(x_{egr}, W_{urea}\right) \le LD_{NH3} \tag{6.11}$$

$$
\begin{aligned}
C_{NOx,step}\left(x_{egr}, W_{urea}\right) &\le LD_{NOx} & M &> 0 \\
C_{NOx,step,idle}\left(x_{egr}, W_{urea}\right) &\le LD_{NOx,idle} & M &\le 0
\end{aligned}
\tag{6.12}
$$

$$C_{\theta_{NH_3,avg,end}}\left(x_{egr}, W_{urea}\right) = \theta_{NH_3,avg,opt} \tag{6.13}$$

The first two constraints, Equations (6.10)-(6.11), are calculated as accumulated values for the prediction horizon, and the third, Equation (6.12), is calculated as a mean value over the control step. A $NO_x$ constraint over the control step is required so that the optimizer does not trade off momentaneous higher $NO_x$ in the beginning of the prediction horizon for lower $NH_3$ slip. The upper bounds of the $NO_x$ and $NH_3$ constraints are set to:

$$LD_{NO_x} = 0.5 \ g/kWh$$

$$LD_{NH_3} = 10 \ ppm$$

During idle operation, where specific $NO_x$ is not defined, a molar fraction constraint bound is used:

$$LD_{NO_x,idle} = 50 \ ppm$$

Note that unlike paper IV, no gradient constraints on $NH_3$ coverage or $NO_x$ conversion are used. The conditioning problems encountered in paper IV were related to that the catalyst temperature was close to equilibrium for an extended period of time. In the MPC optimization problem, similar conditioning problems rarely occurs because the catalyst temperature is typically not at equilibrium at the end of the prediction horizon (the less strict average $NH_3$ coverage constraint does not demand temperature equilibrium). If the system does approach steady state, it is possible to reduce the MPC optimization problem to fewer variables in order to get a more well behaved solution.

In order to determine the prediction horizon, first a characteristic time constant for each catalyst tank is calculated (assuming that each tank is approximated with a first order system):

$$\tau_{MPC,k} = N_c \frac{\theta_{NH_3,ss,k} - \theta_{NH_3,k}}{4 \cdot \Delta r_{ads/des,k}} \tag{6.14}$$

where $\theta_{NH3,k,ss}$ is the steady state $NH_3$ coverage for tank k. $N_c$ is the specific $NH_3$ storage capacity (number of sites) of the catalyst. The steady state coverage is estimated using the current (transient) second layer concentrations and $NH_3$ coverage. The reaction rate for adsorption/desorption is given by:

$$\Delta r_{ads/des,k} = r_{2,k} - r_{3,k} - 2r_{4,k} \tag{6.15}$$

where the reaction rates are given by Equations (4.7)-(4.9). Reaction 5, Equation (4.10), $NH_3$ oxidation is neglected; the influence on the resulting time constant is negligible at the exhaust temperatures provided by the engine. A time constant for the entire catalyst (average $NH_3$ coverage) is introduced, approximating the catalyst with a first order system. It is calculated by weighting the values for each tank together:

$$\tau_{MPC,avg} = \frac{\sum_1^6 \dfrac{d\theta_{NH_3,k}}{dv}}{\sum_1^6 \dfrac{1}{\tau_{MPC,k}} \dfrac{d\theta_{NH_3,k}}{dv}} \tag{6.16}$$

The differential $\dfrac{d\theta_{NH_3,k}}{d\nu}$ is a measure on how fast the $NH_3$ coverage in tank k is changed by a perturbation in feed $NH_3/NO_x$ stoichiometry. This relation can be calculated analytically by differentiating the $NH_3/NO_x$ stoichiometry $\nu$.

The prediction horizon length is chosen to twice the total time constant, i.e:

$$t_{MPC} = 2 \cdot \tau_{MPC,avg} \tag{6.17}$$

The limit of the equality constraint $\theta_{NH_3,avg,opt}$, Equation (6.13), is determined by solving an additional optimization problem similar to the steady state case (Equations (6.1)-(6.4)). As discussed earlier, the catalyst temperature is not at equilibrium at the end of the prediction horizon; the end value limit of the constraint must therefore be calculated based on the current temperature profile of the catalyst.

Also, the optimum injection timing, EGR rate and urea dosing, as given by the steady state optimization, does not necessarily fulfil the constraints at the current catalyst temperature nor provides the lowest possible BSFC. One example where reduced BSFC is possible is during a negative load transient; the catalyst temperature will be at a higher level than in steady state allowing higher engine out $NO_x$ (lower EGR rate) and therefore (in most cases) lower BSFC. The end value optimization problem is simplified by using EGR rate and urea dosing only as optimization variables. Using the simplified steady state solution of the SCR model (Section 4.4.2), the optimization time is negligible compared to the MPC optimization problem (Equations (6.9)-(6.13)).

The urea dosing initial values are compensated for the difference between initial and optimized end value $NH_3$ coverages:

$$W_{urea,init} = W_{urea,ss} + \frac{M_{urea} \cdot \sum_{n=1}^{N} w_{k,n} \cdot N_c \cdot \max\left(0, \theta_{NH_3,avg,opt} - \theta_{NH_3,init}\right)}{2 \cdot x_{M,urea} \cdot t_{MPC}} \tag{6.18}$$

where $x_{M,urea}$ is the mass fraction urea of the aqueous solution. The second part of Equation (6.18) is simply the requested increase in $NH_3$ mass (compensated for $NH_3$ content in the urea solution) divided by the prediction horizon length.

The control step length is 1 s and the maximum number of iterations is limited to 10 in the results section below. Using a shorter control step will provide slightly better results at the expense of longer computational time. Considering that solving each MPC optimization problem takes ~20-60 s, increasing the computational load is not a viable option.

The choice of optimization routine is thoroughly discussed in paper IV. All optimization work in this thesis uses the SNOPT large scale non-linear optimizer [38] which is based on Sequential Quadratic Programming (SQP).

### *6.4.2 Step Response Results*

In order to illustrate how the MPC application works, the controller is applied to the positive load transient discussed in Section 6.3.1. The results are presented in Figure 6.5. Note that the catalyst will approach steady state in this step response experiment (unlike in the WHSC/WHTC). Therefore an exception is made in the MPC optimization problem when the prediction horizon is very short (<5 s); the problem is reduced to two variables which are held constant over the prediction horizon.

As a comparison, the results using urea dosing and EGR calculated from the optimum steady state calibration (denoted SS) are also given. The SS calibration uses the torque and speed inputs only and does not consider the dynamics of the catalyst. Note that peak $NH_3$ slip is reduced by an order of magnitude using MPC, and specific $NO_x$ is almost perfect at the constraint limit of 0.5 g/kWh throughout the step response (Figure 6.5).

During the first 30 s, the catalyst is at steady state (equalling the initial values). When the load increases from 600 to 2300 Nm at 30 s, the MPC controller switches the urea dosing off in order to avoid (future) $NH_3$ slip by decreasing the $NH_3$ coverage. At this point, the prediction horizon is quite long (~50 s) due to the substantial deviation from steady state $NH_3$ coverage and low temperature/reaction rates (Figure 6.5). The urea flow remains zero up to ~95 s, then it starts to approach the steady state value. The EGR rate is reduced to a lower level than steady state between ~40-95 s; this will consume $NH_3$ from the surface and further decrease the $NH_3$ coverage. Note that even though the actions taken by the controller to decrease $NH_3$ slip is successful, the constraint limit of 10 ppm is violated (peak $NH_3$ slip is 22 ppm); all constraints cannot be met in this case. Depending on the weights chosen on the constraints, the balance between violating the different constraints is set. In the MPC implementation presented in this thesis, higher weights are used on the specific $NO_x$ constraints than the $NH_3$ slip constraint; this is related to the fact that only average $NH_3$ slip is limited in the legislation. Based on experience, temporarily violating the NH3 slip constraint is a less significant problem than violating the $NO_x$ constraint during the control step.

The $NH_3$ coverage at two different axial positions is also presented in Figure 6.5. In the SS case, it is obvious how the stored $NH_3$ from the first part of the catalyst is released and moves further down the catalyst. Also note the close correlation between $NH_3$ coverage at the catalyst outlet and $NH_3$ slip. Using MPC, $NH_3$ coverage in the beginning of the catalyst is reduced to almost zero after ~90 s, resulting in less $NH_3$ which can be released from the surface and progress down the catalyst. The significant reduction in $NH_3$ coverage at the catalyst outlet (with the MPC controller) correlates well with the decrease in $NH_3$ slip.
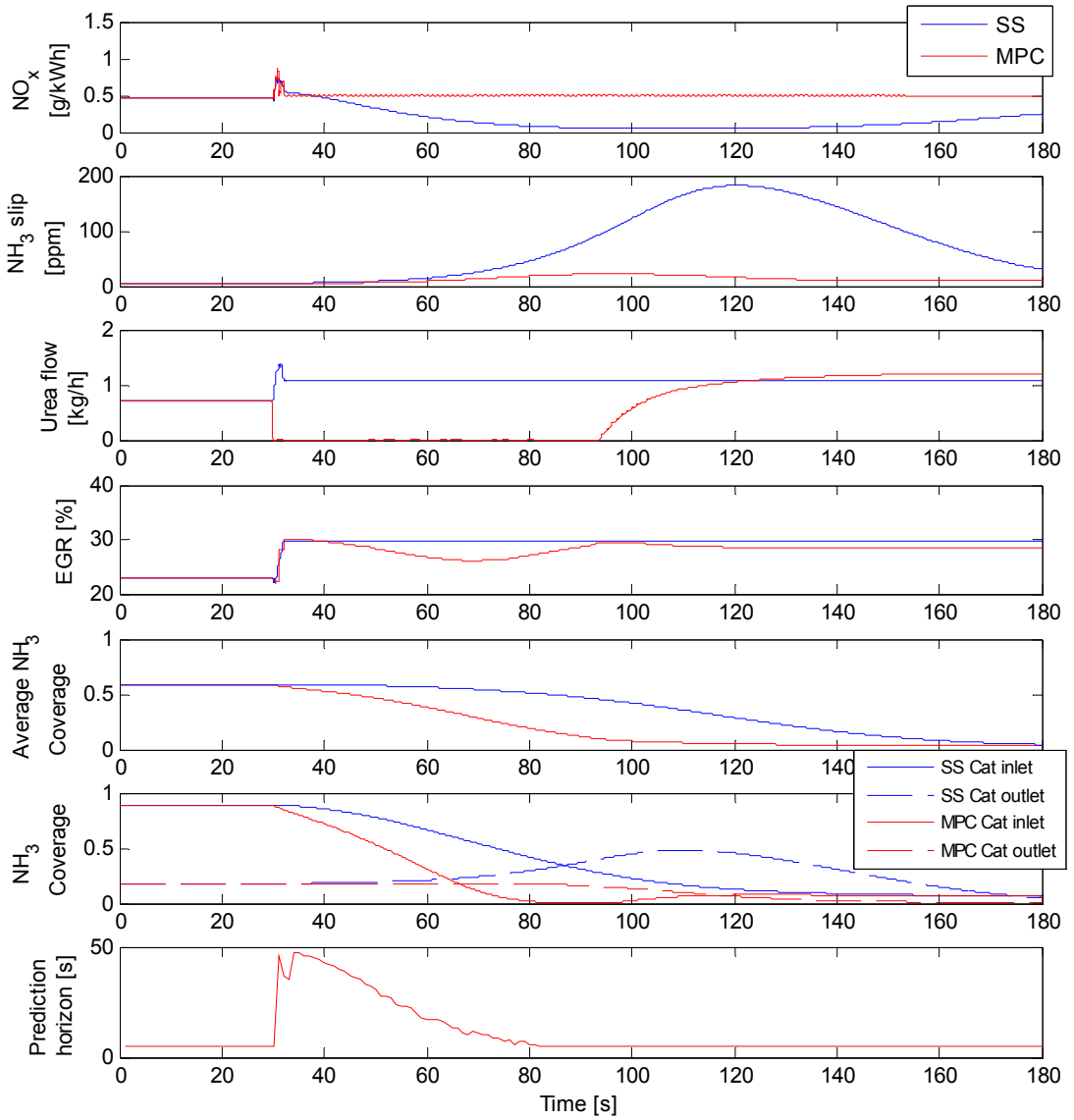
**Figure 6.5 Optimization results, positive load transient 600-2300 Nm at 1300 rpm.**

### *6.4.3 WHSC Results*

Excellent results can be achieved with MPC on a World Harmonized Stationary Cycle (WHSC) (Table 6.1). Using MPC, specific $NO_x$ is reduced to below the target and the peak $NH_3$ slip is substantially reduced, while fuel consumption is unchanged compared to the SS case. As a comparison, the results of a steady state calibration optimized for 0.3g/kWh $NO_x$ is also given in Table 6.1; both the $NO_x$ and average $NH_3$ slip constraints can be met with this approach. The peak $NH_3$ slip (which is currently not regulated) is substantially higher than with the MPC however. Note that the BSFC minimum is broad – the difference between the first three cases is less than 0.05%. Another comparison is included in Table 6.1; the steady state calibration optimized for the lowest possible $NO_x$ during all operating conditions. The peak NH3 slip is on the same level as with the MPC, although at a substantial increase in fuel consumption (2.8%).

**Table 6.1 Optimization results, WHSC.**

|  | $NO_x$ [g/kWh] | $NO_x$ engine out [g/kWh] | $NH_3$ slip [ppm] | $NH_3$ slip peak [ppm] | BSFC [norm] |
|---|---|---|---|---|---|
| **SS** | 0.64 | 4.09 | 9.71 | 85.4 | 100.0 |
| **MPC** | 0.46 | 3.43 | 4.02 | 17.2 | 100.0 |
| **SS 0.3g/kWh** | 0.46 | 3.46 | 10.0 | 74.2 | 100.0 |
| **SS min. $NO_x$** | 0.34 | 1.21 | 2.45 | 14.2 | 102.8 |

With the MPC, urea dosing is active during both idle sequences, i.e. WHSC step one and thirteen (defined in Table 1.1) in order to meet the $NO_x$ constraints, Equations (6.10) and (6.12). At steady state idle, the exhaust temperature is too low to allow urea dosing which is not the case in the test cycle due to heat transfer from the exhaust system. Note that the average $NH_3$ coverage increases during the first idle step with the MPC. The increase will continue during the positive load transient (ramp) between step one and two (210-230 s) up to the constraint limit of 0.75. This will increase $NO_x$ conversion substantially during this time sequence compared to the steady state calibration. Subsequently, the high $NH_3$ coverage will result in $NH_3$ slip due to the increasing temperature during step two. This is compensated for by the MPC by decreasing the EGR rate and urea dosing between ~280-350 s.

The NH$_3$ slip peak of 85 ppm in the SS case is compensated for in a similar manner by reducing the EGR rate and turning off the urea dosing between ~650-690 s (Figure 6.6). This will rapidly decrease the NH$_3$ coverage. In general, the EGR level is increased with the MPC, which explains the decreased engine out NO$_x$ (Table 6.1).
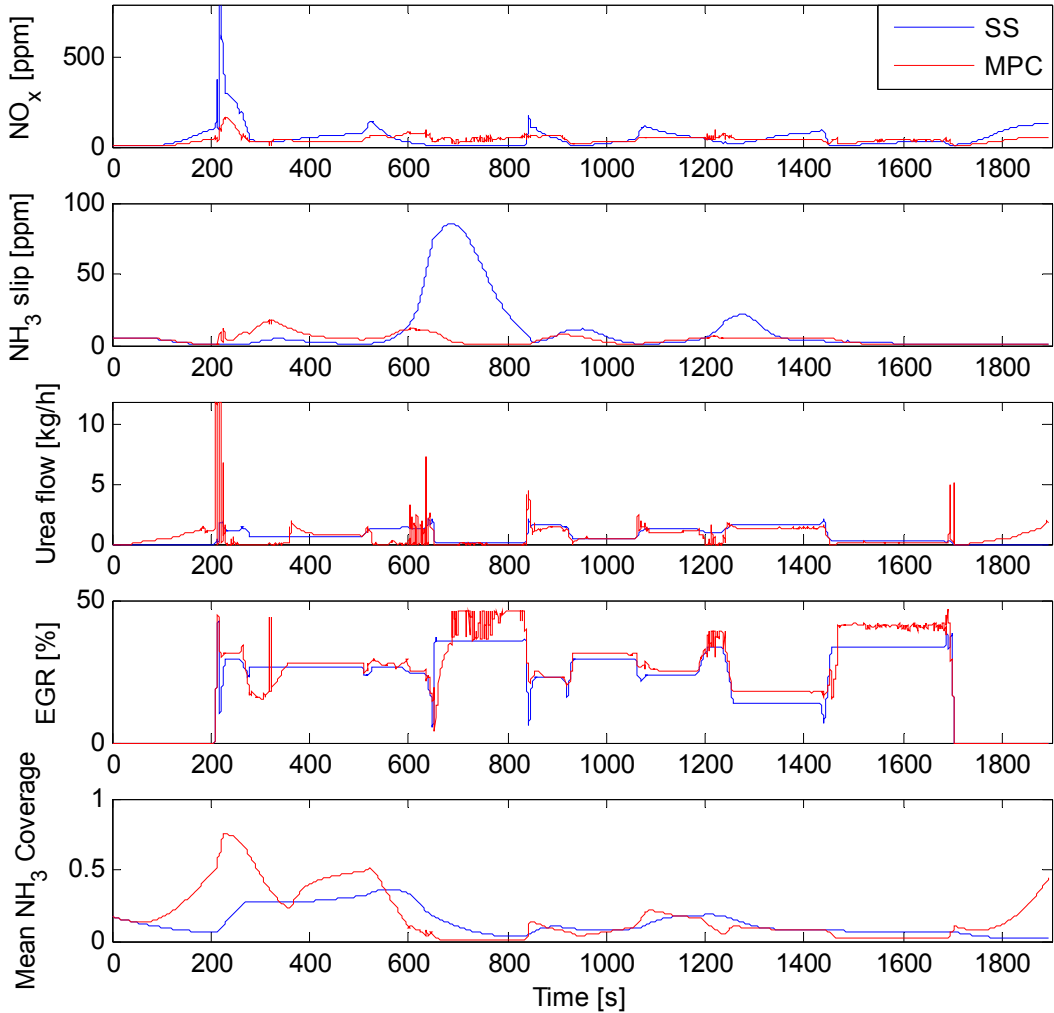


**Figure 6.6 Optimization results, WHSC.**

### *6.4.4    Warm Start WHTC Results*

The initial conditions for the warm start WHTC is calculated by running the cold start WHTC followed by a hot soak period of 5 minutes (when the engine is turned off, i.e. the exhaust flow is zero). The hot soak period results in a decrease in exhaust system temperature whereas the catalyst temperature remains unchanged; external heat transfer from the catalyst is neglected in the model. This is a reasonable assumption however considering that the catalyst is situated inside a silencer which acts as an efficient insulator. In order to meet the emission targets in the WHTC, the MPC must use more strict constraints than in the WHSC. For reasons discussed in paper V, the $NO_x$ upper bounds in the constraints are altered to:

$LD_{NOX}=0.25 \ g/kWh$

$LD_{NOX,idle}=5 \ ppm$

The results of the optimization are given in Table 6.2, Figure 6.7 and Figure 6.8. The steady state calibration results in specific $NO_x$ and $NH_3$ slip higher than the target ones and an unacceptably high peak $NH_3$ slip level. Using the MPC, all constraints can be met, although at the expense of an increase in fuel consumption of 0.9%. Analogous to the WHSC optimization, overall engine out $NO_x$ is reduced using higher EGR levels. This explains the increase in BSFC. As a comparison, the results of a steady state calibration optimized for 0.1g/kWh $NO_x$ is also given in Table 6.2. The $NO_x$ and average $NH_3$ slip constraints can be met with this calibration, although the peak $NH_3$ slip is over 100 ppm and the fuel consumption is increased by 2.4%. Using a steady state calibration optimized for the lowest possible $NO_x$, peak $NH_3$ slip can be reduced to 66 ppm at the expense of a 3.6% increase in BSFC (Table 6.2).

**Table 6.2 Optimization results, warm start WHTC.**

|  | $NO_x$ [g/kWh] | $NO_x$ engine out [g/kWh] | $NH_3$ slip [ppm] | $NH_3$ slip peak [ppm] | BSFC [norm] |
|---|---|---|---|---|---|
| **SS** | 1.20 | 4.43 | 13.5 | 153 | 100.0 |
| **MPC** | 0.49 | 2.53 | 5.28 | 46.9 | 100.9 |
| **SS 0.1g/kWh** | 0.42 | 1.68 | 9.00 | 102 | 102.4 |
| **SS min. $NO_x$** | 0.37 | 1.39 | 7.46 | 66.0 | 103.6 |

Looking at the time resolved results of the first third of the WHTC shown in Figure 6.7, the main difference apart from consistently higher EGR rates is the high urea flow during the first ~15 s of the test cycle. The results are rapid increases in $NH_3$ coverage and $NO_x$ conversion.
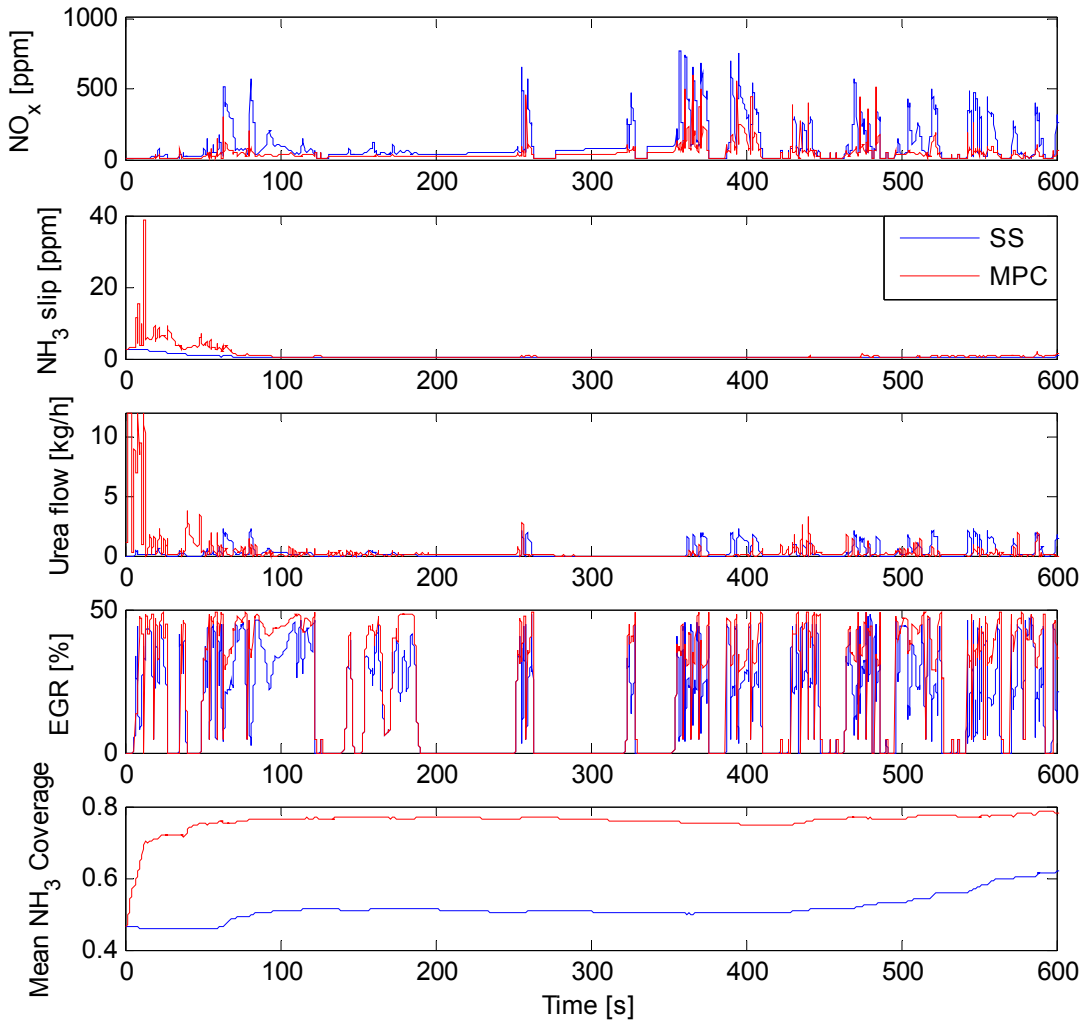


**Figure 6.7 Optimization results, sequence of the warm start WHTC.**

The optimization results of the last 600 s of the warm start WHTC are given in Figure 6.8. The $NH_3$ slip peak at ~1480 s is decreased by the MPC by (nearly) turning off the urea injection between 1325-1510 s. Note that contrary to the general trend, the EGR rate is reduced compared to the steady state calibration in order to reduce $NH_3$ slip around 1460-1500 s. Still, the constraint limit of 10 ppm is violated; it is not possible to meet all the constraints during this time sequence.
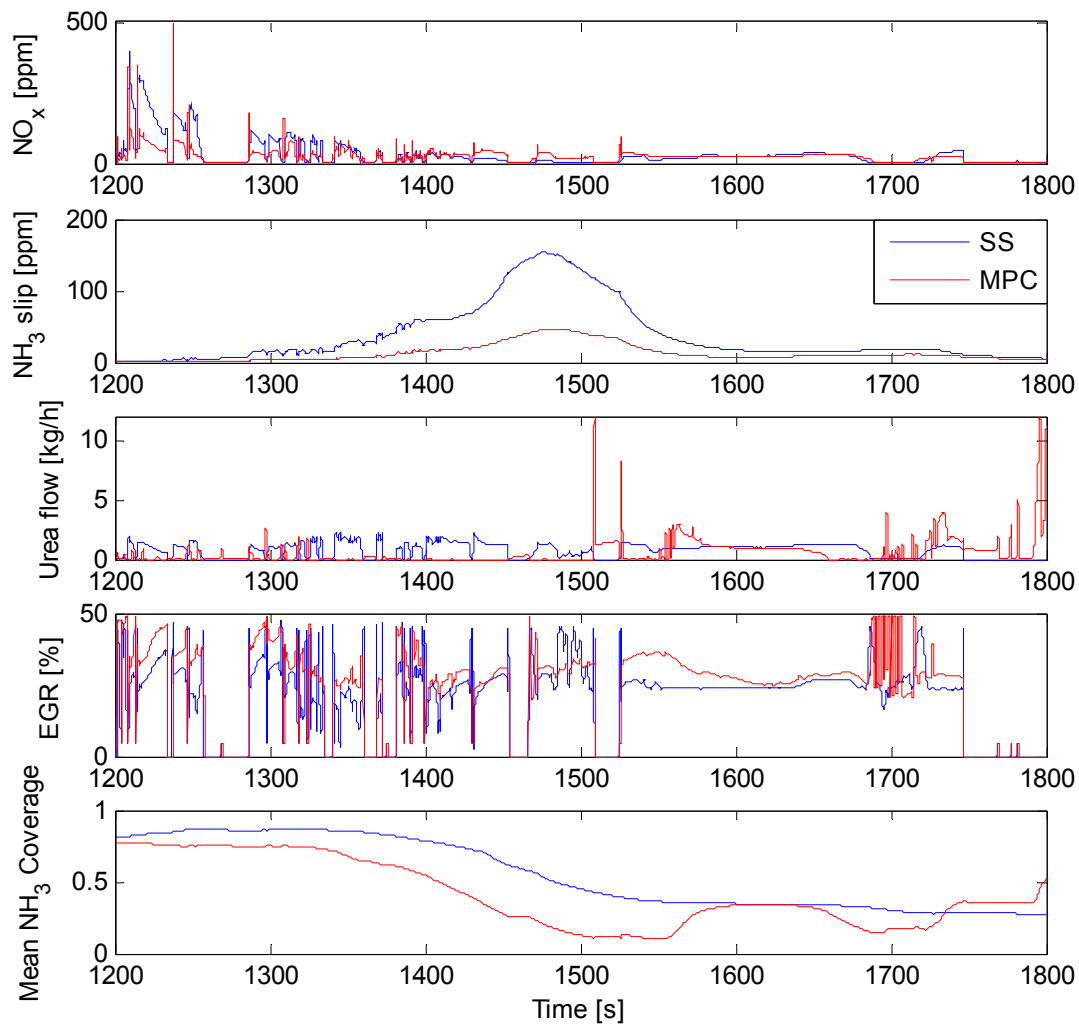


**Figure 6.8 Optimization results, sequence of the warm start WHTC.**

### *6.4.5 Cold Start WHTC Results*

The initial $NH_3$ coverage states for the cold start WHTC are set to the optimum $NH_3$ coverage profile following the warm started cycle. The temperature states all equal the ambient temperature (298 K). Using the same constraints as in the warm start case yields the results given in Table 6.3. Note that no active measures such as intake throttling (as discussed in the future work chapter) have been taken to increase exhaust temperature. This is further discussed in the future work chapter. Neither the MPC nor the 0.1g/kWh steady state calibration fulfil all constraints. Assuming a weighting factor of 1/7, i.e. the weighted emissions are calculated as 1/7 times the cold start cycle emissions plus 6/7 times the warm start cycle emissions; the result using the MPC is slightly above the target; 0.52 g/kWh $NO_x$.

**Table 6.3 Optimization results, cold start WHTC.**

|  | $NO_x$ [g/kWh] | $NO_x$ engine out [g/kWh] | $NH_3$ slip [ppm] | $NH_3$ slip peak [ppm] | BSFC [norm] |
|---|---|---|---|---|---|
| **SS** | 1.48 | 4.43 | 12.6 | 152 | 100.0 |
| **MPC** | 0.71 | 2.51 | 4.83 | 46.3 | 101.0 |
| **SS 0.1g/kWh** | 0.57 | 1.68 | 9.03 | 95.2 | 102.4 |

The time resolved results for the first third of the WHTC are shown in Figure 6.10. Note that no urea dosing is possible during the first ~400 s due to the low exhaust temperature. During this period, the average $NH_3$ coverage is fairly constant at the initial value; the catalyst temperature is low resulting in negligible $NO_x$ conversion and correspondingly low $NH_3$ consumption. As the exhaust temperature increases, a large amount of urea is injected in order to increase the $NH_3$ coverage (up to the constraint limit of 0.75 at 600 s) and increase the $NO_x$ conversion. The EGR rate is overall higher with the MPC resulting in lower $NO_x$ even before urea injection is possible. The remaining part of the WHTC, 600-1800 s, will be close to identical to the warm start case. A comparison of the catalyst temperature is given in Figure 6.9; note the convergence after ~700 s.
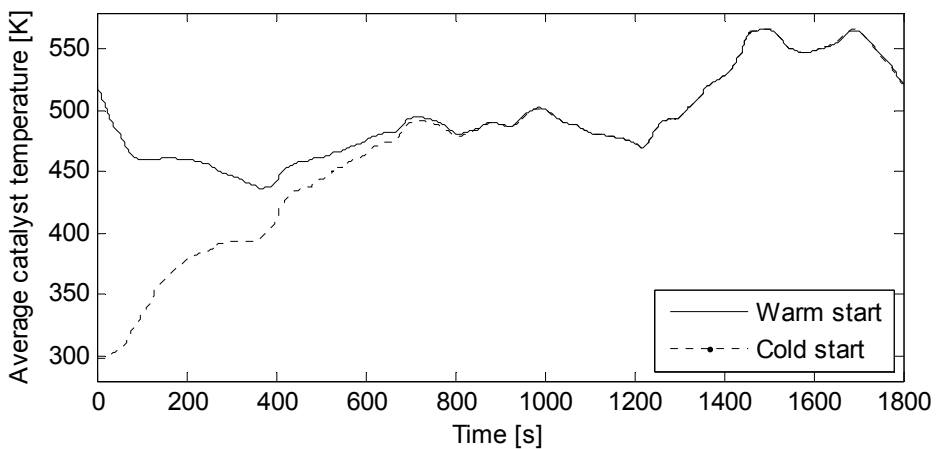


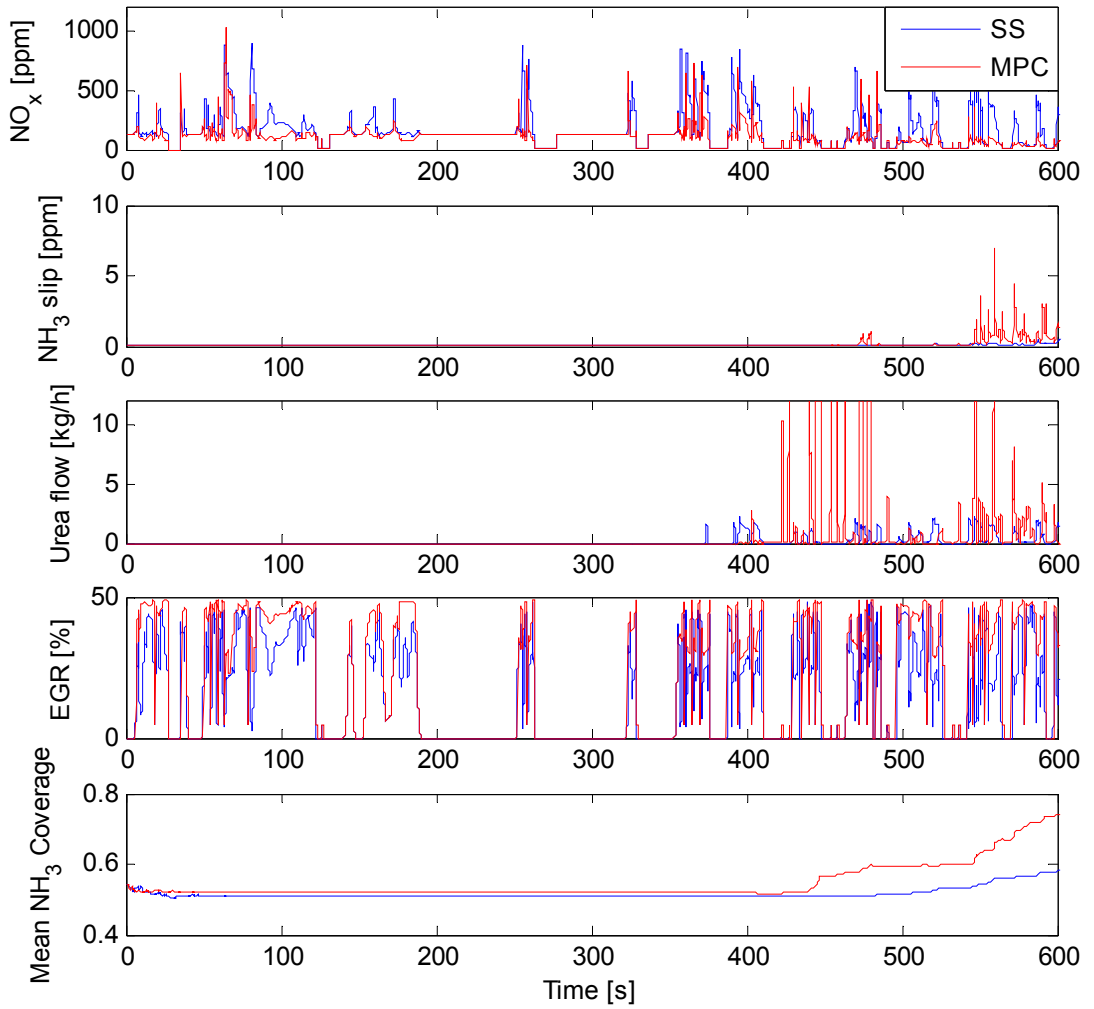**Figure 6.9 Catalyst temperature, cold and warm started WHTC.**

**Figure 6.10 Optimization results, sequence of the cold start WHTC.**

# 7   Summary

The first half of the thesis work involved developing computationally efficient models of diesel engine combustion, gas exchange in a diesel engine, the exhaust system and $NO_x$ reduction using a SCR catalyst. All models are implemented in Matlab Simulink.

The combustion model is of the zero dimensional type. The cylinder contents are divided into one unburned zone consisting of air and recirculated exhaust gas and one burned zone containing the combustion results. The model is predictive, i.e. the heat release rate is predicted using fuel injection parameters. The burned zone temperature is calculated in two steps, first assuming perfect combustion, and secondly compensating this value for dissociation using tabulated data. $NO_x$ formation is calculated according to the original Zeldovich mechanism. Tabulated data describing the equilibrium concentrations in the burned zone are used to speed up calculations. The simulation time is ~8 ms per cycle on a 2.67 GHz CPU.

In addition to the combustion model, a gas exchange model of the quasi-steady filling and emptying type is presented. A total of 4 states are used to describe the gas flows and temperatures in the diesel engine. The modelled engine includes an EGR system and a variable geometry turbocharger (VGT). The model requires a 10 ms time step length to remain stable in all conditions, but is extremely fast due to an efficient Simulink implementation.

The exhaust system model describes convective heat transfer between the exhaust gas, exhaust system and the surrounding air. A single temperature state is used to model the wall temperature.

The SCR catalyst model is based on a state space concept. The catalyst is discretized into six continuously stirred tanks in the axial direction, and two wall layers are used to describe the mass transfer in the porous catalyst wall. Eley-Rideal kinetics is applied to calculate the reaction rates on the catalyst surface. At low temperatures the model uses an implicit method of calculating the $NH_3$ coverage differential. At higher temperatures, the model is simplified to a first order system using an operating condition dependent characteristic time constant. These simple, yet robust methods allow for long step lengths in the process of solving the differential equations. Using a 0.5 s time step, the computational performance is ~500 times real time.

By combining all sub models, the result is a complete model which can be used to study the effects of varying EGR rate, injection pressure, injection timing and urea injection on $NO_x$ formation and overall fuel/urea consumption.

The complete model is used for model based optimization. The optimization problem is formulated to minimize brake specific fuel consumption including urea cost while maintaining $NO_x$ and $NH_3$ emissions at Euro VI levels. The steady state optimization problem is solved in an efficient manner by using a simplified steady state solution of the SCR catalyst model. The highest $NO_x$ conversion (>90%) is achieved at low speeds and high torque. At higher speeds, the conversion is limited by excessive space velocities and at low loads the limitation is temperature.

The challenges of transient operation of the system are characterized. Three critical operating sequences are identified:

1. Positive load transient

2. Negative load transient

3. Cold start

In case 1, the main challenge is to keep the $NH_3$ slip at a low level despite the increasing catalyst temperature. The opposite problem is identified in case 2; insufficient $NO_x$ reduction due to the decreasing catalyst temperature and corresponding higher $NH_3$ coverage equilibrium. The third case is similar to case 1 except for that no urea injection is initially possible due to the low exhaust temperature.

A non linear MPC is developed to solve the optimization problem for transient sequences. The prediction horizon length is calculated based on the current $NH_3$ coverage and the reaction rate for $NH_3$ adsorption/desorption. An equality constraint on the average $NH_3$ coverage at the end of the prediction horizon is introduced in order to reach the optimum state considering the temperature profile of the catalyst. A SQP-based optimization routine is used to solve the MPC optimization problem in each time step.

The MPC is applied to the certification test cycles (WHSC/WHTC). In the WHSC, the targets of 0.5 g/kWh $NO_x$ and 10 ppm average $NH_3$ slip are achieved and the peak $NH_3$ slip is reduced substantially while the fuel consumption is unchanged compared to the optimum steady state calibration. Equally good results are achieved in the WHTC with emissions lower than the target. Compared to a conservative steady state calibration with $NO_x$ and average $NH_3$ emissions on the same level, peak $NH_3$ slip is reduced from 102 to 47 ppm, and fuel consumption is improved by 1.5%.

# 8   Future Work

One of the most interesting extensions of this work is to use the MPC in combination with look-ahead. With knowledge of the future load/speed profiles, even better performance could probably be achieved. Using look-ahead in the certification test cycles is of course not an option; this would be considered "cycle beating". It would be possible however to use a more conservative emission strategy when no look-ahead information is available and a more aggressive strategy during real world driving where GPS information is available.

Optimization of cold start sequences is not treated as a special case in this work. Improved emissions in the cold start WHTC can be achieved by using an alternative approach at low catalyst temperatures where active measures are taken to increase the exhaust temperature. Such measures, for example using intake throttling and retarded injection timing does generally result in higher fuel consumption however. Retarded injection also results in lower $NO_x$ engine out.

Currently, the MPC is not executable in real time even on a powerful PC. One of the key factors to achieve faster performance is the optimization routine. The SQP optimizer used requires a large number of function evaluations. More work is needed in the optimization area to find a more suitable and efficient optimization routine. Possibly further simplifications of the SCR catalyst model are also needed in order to reach real time performance.

# 9   References

1.  J. W. Girard, C. Montreuil, J. Kim et al., "Technical Advantages of Vanadium SCR Systems for Diesel NOx control in Emerging Markets", SAE Technical Papers 2008-01-1029, 2008.

2.  www.dieselnet.com, Technology Guide / Emissions Standards, 2009-04-07.

3.  N. Ladommatos, S. M. Abdelhalim, H. Zhao and Z. Hu, " The Dilution, Chemical and Thermal Effects of Exhaust Gas Recirculation on Diesel Engine Emissions – Part 4: Effects of Carbon Dioxide and Water Vapour", SAE Technical papers 971660, 1997.

4.  J. E. Dec, "A Conceptual Model of DI Diesel Combustion Based on Laser Sheet Imaging", SAE Technical papers 970147, 1997.

5.  F. G. Chmela and G. C. Orthaber, "Rate of Heat Release Prediction for Direct Injection Diesel Engines Based on Purely Mixing Controlled Combustion", SAE Technical papers 1999-01-0186, 1999.

6.  F. G. Chmela, M. Engelmayer, G. Pirker and M. Wimmer, "Prediction of Turbulence Controlled Combustion in Diesel Engines", Proceedings of THIESEL 2004 Conference on Thermo- and Fluid Dynamic Processes in Diesel Engines, 2004.

7.  G. Pirker, F. G. Chmela and A. Wimmer, "ROHR Simulation for DI Diesel Engines Based on Sequential Combustion Mechanisms", SAE Technical papers 2006-01-0654, 2006.

8.  R. Egnell, "Combustion Diagnostics by Means of a Multizone Heat Release Analysis and NO Calculation, SAE Technical Papers 981424, 1998.

9.  R. Egnell, "A Theoretical Study of the Potential of NOx reduction by Fuel Rate Shaping in a DI Diesel Engine", SAE Technical Papers 2000-01-2935, 2000.

10. R. Egnell, "On Zero-dimensional Modelling of Combustion and $NO_x$ Formation in Diesel Engines", Doctoral Thesis, Division of Combustion Engines, Department of Heat and Power Engineering, Lund Institute of Technology, Lund, 2001.

11. M. Andersson, C. Nöhre, B. Johansson and A. Hultqvist, "A Predictive Real Time $NO_x$ Model for Conventional and Partially Premixed Diesel Combustion", SAE Technical Papers 2006-01-3329, 2006.

12. M. Andersson, "Fast $NO_x$ Prediction in Diesel Engines", Licentiate Thesis, Division of Combustion Engines, Department of Energy Sciences, Lund Institute of Technology, 2006.

13. R. M. Siewert, "A phenomenological Engine Model for Direct Injection of Liquid Fuels, Spray Penetration, Vaporization, Ignition Delay and Combustion", SAE Technical Papers 2007-01-0673, 2007.

14. J. B. Heywood, "Internal Combustion Engine Fundamentals", McGraw-Hill Series in Mechanical Engineering, 1988, pp. 679-680, 572-577, 907-910.

15. R. J. Kee, F. M. Rupley and J.A. Miller, "The Chemkin Thermodynamic Data Base", Sandia report, SAND87-8215B, 1990.

16. C. Ericson, "Mean Value Modeling of a Poppet Valve EGR-System", Master's thesis, Vehicular Systems, Department of Electrical Engineering, Linköping University, 2004.

17. C. Ericson, "$NO_x$ Modelling of a Complete Diesel Engine / SCR System", Licentiate thesis, Division of Combustion Engines, ISRN LUTMDN/TMHP-07/7047, Department of Energy Sciences, LTH, Lund University, 2007.

18. C. M. Schär, C. H. Onder, M. Elsener and H. P. Geering, "Model-based Control of an SCR System for Mobile Application", F2004V205 Proceedings of World Automotive Congress, FISITA 2004, 2004.

19. L. Eriksson, "Mean Value Models for Exhaust System Temperatures", SAE Technical Papers 2002-01-0374, 2002.

20. E. Tronconi and P. Forzatti, "Adequacy of Lumped Parameter Models for SCR Reactors with Monolith Structure", AlChe Journal 38, 1992.

21. L. Andersson, P. Gabrielsson and I. Odenbrand, "Reducing $NO_x$ in Diesel Exhausts by SCR Technique: Experiments and Simulations", A.I.Ch.E. Journal 40 Issue 11 (1994) 1911-1919.

22. L. Andersson, "Mathematical Modelling in Catalytic Automotive Pollution Control", Doctoral Thesis, Department of Chemical Reaction Engineering, Chalmers University of Technology, 1995.

23. D. Chatterjee, T. Burkhardt, B. Bandl-Konrad, T. Braun, E. Tronconi, I. Nova and C. Ciardelli, "Numerical Simulation of Ammonia SCR-Catalytic Converters: Model Development and Application", SAE Technical Papers 2005-01-0965, 2005.

24. I. Nova, C. Ciardelli, E. Tronconi, D. Chatterjee and B. Bandl-Konrad, "$NH_3$-NO/$NO_2$ Chemistry Over V-based Catalysts and Its Role in the Mechanism of the Fast SCR Reaction", Catalysis Today 114 (2006) 3-12, 2006.

25. D. Chatterjee, T. Burkhardt, M. Weibel, E. Tronconi, I. Nova and C. Ciardelli, "Numerical Simulation of NO/$NO_2$/$NH_3$ Reactions on SCR-Catalytic Converters: Model Development and Applications", SAE Technical Papers 2006-01-0468, 2006.

26. B. Westerberg, "Transient Modelling of a HC-SCR Catalyst for Diesel Exhaust Aftertreatment", Chemical Engineering Journal 92 (2003) 27-39, 2003..

27. M. Devarakonda G. Parker, J. H. Johnson, V. Strots and S. Santhanam, "Adequacy of Reduced Order Models for Model-Based Control in a Urea-SCR Aftertreatment System", SAE Technical papers, 2008-01-0617, 2008.

28. L. Lietti, I. Nova, E. Tronconi and P. Forzatti, "Transient kinetic study of the SCR-DeNOx reaction", Catalysis Today 45 (1998) 85-92, 1998.

29. D. Murzin and T. Salmi, "Catalytic Kinetics", Elsevier, Amsterdam, 2005, pp. 285-288, 408, 406.

30. D. Chatterjee, T. Burkhardt, T. Rappe, A. Güthenke and M. Weibel, "Numerical Simulation of DOC+DPF+SCR Systems: DOC Influence on SCR Performance", SAE Technical Papers 2008-01-0867, 2008.

31. R. B. Bird, W. E. Stewart, E. N. Lightfoot, "Transport phenomena", John Wiley & Sons, Singapore, 1960, pp. 542-546.

32. H. S. Fogler, "Elements of Chemical Reaction Engineering", Prentice Hall PTR, 2000, pp. 967.

33. D. Upadhyay, M. Van Nieuwstadt, "Model Based Analysis and Control Design of a Urea-SCR deNOx Aftertreatment System", ASME Journal of Dynamic Systems, Measurement and Control, 128, 2006.

34. M. Devarakonda G. Parker, J. H. Johnson, V. Strots and S. Santhanam, "Model-Based Estimation and Control System Development in a Urea-SCR Aftertreatment System", SAE Technical papers, 2008-01-1324, 2008.

35. J. N. Chi and H. F. M. Dacosta, "Modeling and Control of a Urea-SCR Aftertreatment System", SAE Technical papers 2005-01-0966, 2005.

36. M. Nikolaou, "Model Predictive Controllers: A Critical Synthesis of Theory and Industrial Needs", Advances in Chemical Engineering Volume 26, 2001, pp. 134.

37. E. Hellström, A. Fröberg and L. Nielsen, "A Real-Time Fuel-Optimal Cruise Controller for Heavy Trucks Using Road Topography Information", SAE Technical papers 2006-01-0008, 2006.

38. Gill P.E., Murray W. and Saunders, M.A., "User's Guide for SNOPT Version 7: Software for Large-Scale Nonlinear Programming", 2007.

# 10 Summary of Papers

## *Paper I*

**Transient emission predictions with quasi stationary models**

C. Ericson, B. Westerberg and R. Egnell

SAE Technical papers 2005-01-3852, 2005

Quasi stationary calculations are applied to measurements from three diesel engines certified for Euro III. $NO_x$ and fuel consumption is reasonably well predicted without any compensation. A transient correction method termed the Delay Model is developed to make time resolved correction of HC and PM emissions. The delay model has a physical interpretation in the sense that it estimates a turbocharger delay time and a corresponding corrected air-fuel equivalence ratio during transient operation. The overall results are satisfactory for predicting on road emissions from heavy duty engine populations, but lacks in accuracy to be used for simulation and optimization purposes.

*The Delay Model was developed by the authors. The measurements were performed by Anders Hedbom at AVL/MTC as a part of the COST 346 project. The paper was written by the main author.*

## *Paper II*

**Modelling diesel engine combustion and $NO_x$ formation for model based control and simulation of engine and exhaust aftertreatment system**

C. Ericson, M. Andersson, R. Egnell and B. Westerberg

SAE Technical papers 2006-01-0687, 2006

A simple and extremely computationally efficient predictive heat release and $NO_x$ formation model is developed. The model uses a zero dimensional two zone concept. The combustion and $NO_x$ formation models involve tabulated data to simplify the calculations. A simple gas exchange model of the filling and emptying type is added which makes the model a complete engine simulation package. The accuracy is excellent, a 10.4 % mean relative error is noted over a series of steady state points, and accumulated $NO_x$ emissions over the ETC is predicted with a 7.1 % relative error.

Correction: the pre exponential factor of Equation 24 should read $1.5 \cdot 10^9$.

*The model was originally developed by Rolf Egnell and improved by the main author. The measurements were performed by Mikael Persson at Scania Engine Development. The paper was written by the main author.*

## *Paper III*

**A state-space simplified SCR catalyst model for real time applications**

C. Ericson, I. Odenbrand and B. Westerberg

SAE Technical papers 2008-01-0616, 2008.

A model of a vanadia based SCR catalyst of typical heavy truck dimensions is developed. The basic model structure is a series of continuously stirred tank reactors using discretized catalyst walls to describe the mass transport. The model uses a state space concept. At low temperatures, an implicit step length is used to calculate the ammonia coverage. At higher temperatures, the model is simplified to a first order system using an operating condition dependent characteristic time constant. Combining these two methods allows for longer time step lengths compared to previous models. The result is an SCR catalyst model of previously unseen computational efficiency. Yet the model shows agreement with measurements on par with more complex models.

*The model in its original form was developed by Björn Westerberg. The methods applied to allow long step lengths were developed by the main author. The measurements were performed by Björn Westerberg at Scania Engine Development. The paper was written by the main author.*

## *Paper IV*

**Characterisation and Model Based Optimization of a Complete Diesel Engine/SCR System**

C. Ericson, R. Egnell, I. Odenbrand and B. Westerberg

SAE Technical papers 2009-01-0896, 2009.

The model of the complete system consisting of engine, exhaust system and SCR catalyst is presented. The predictive heat release part of the engine model is thoroughly reworked from paper II. The complete model is validated using transient test cycle experiments (ETC) measured in the engine test bed. Three critical operating sequences are identified: positive load transient, negative load transient and cold start. An optimization problem is presented in order to perform model based optimization of the three critical sequences. The optimization problem studied is targeted at minimizing fuel consumption (including Urea cost) while achieving Euro 6 emission levels ($NO_x$ and $NH_3$ slip) and not exceeding the design limits of the engine. The conclusion is that improvements in emissions can be achieved by simultaneously optimizing engine out $NO_x$ and Urea dosing while maintaining good fuel economy.

Correction: Incorrect initial values for the SCR catalyst model were used during validation of the model. This explains the high deviation in specific tailpipe $NO_x$ compared to the results in paper V.

*All modelling and optimization work was done by the main author. The measurements used for calibration and validation of the model were performed by Magnus Andersson and Björn Westerberg at Scania Engine Development. The paper was written by the main author.*

## *Paper V*

### Model Predictive Control of a Combined EGR/SCR HD Diesel Engine

C. Ericson, R. Egnell, I. Odenbrand and B. Westerberg

Abstract submitted to SAE World Congress 2010.

The optimization problem in paper IV is further studied. First, a steady state optimization of the whole operating range of the engine is performed. Transient optimization is handled using Model Predictive Control (MPC). A number of simplifications to the optimization problem and models make the MPC feasible. The MPC shows great improvements in emissions in both the WHSC and WHTC, achieving the target of 0.5 g/kWh $NO_x$ and 10 ppm $NH_3$ slip. Compared to a more conservative steady state calibration with $NO_x$ emissions on the same level, peak $NH_3$ slip is reduced substantially, and fuel consumption is improved with 1.5% in the WHTC.

The latest version of the complete model is presented in the appendix, including a validation part. The main differences from paper IV are a further improved predictive heat release model and a simplified method to find the steady state solution of the SCR catalyst model.

*All modelling and optimization work was done by the main author. The measurements used for calibration and validation of the model were performed by Magnus Andersson and Björn Westerberg at Scania Engine Development. The paper was written by the main author.*